

Overburden subsidence and sinkholes

Authors: Prof. Dr. habil. Heinz Konietzky, M. Sc. Stefan Harms
(TU Bergakademie Freiberg, Geotechnical Institute)

1	Introduction.....	2
2	Types of mining induced surface damages	2
3	Continuous subsidence	4
	Fundamentals	4
	Profile functions	8
	Influence functions	10
4	Influence of geological effects and mining parameters.....	13
5	Discontinuous subsidence.....	15
	Empirical models.....	15
	Analytical models	16
	5.1.1 Volume balance models.....	16
	5.1.2 Simple geomechanical models	20
6	Consequences of mining induced surface movements	30
	Static ground movements	30
	Time-dependent ground movements	32
7	Numerical Models.....	34
	Example 1: Numerical simulation of continuous subsidence above an underground coal mine.....	34
	Example 2: Numerical simulation of sinkhole with an continuum approach (Shiau et al., 2016).....	38
	Example 3: Numerical simulation of sinkhole with a discontinuum approach (Coudron et al., 2006)	39
	Example 4: Numerical simulation of sinkhole over brine-filled caverns with a discontinuum approach (Minkley & Lüdeling, 2020).....	41
	Example 5: Numerical simulation of sinkhole using a particle based approach discontinuum approach (Song & Konietzky, 2019)	43
8	References	44

1 Introduction

Surface movements and deformations like settlements, inclinations or even sinkholes can be caused by human activities (e.g. mining, petroleum engineering) or natural underground processes (leaching processes, erosion, suffosion etc.). Potential consequences of such deformations are damages on buildings and infrastructure but also hazard for human beings. This chapter considers only mining related subsidence phenomena. Nevertheless, most of the below given information is also applicable to natural induced deformation processes.

2 Types of mining induced surface damages

The type of subsidence depends on various factors. In case of brittle overburden above a near-surface excavation, a basin can be formed with step like edges. As shown in Fig. 1 oblique shear fractures (green) as well as fractures perpendicular to the stratification (orange) can occur. In case of a compact overlying rock mass above deep and large underground mining excavations, a subsidence trough will appear (Fig. 2) which extends beyond the mining claim boundaries.

If the overburden consists of loose soil, a wedge-shaped depression can be formed, which has the shape of a funnel and narrows with ongoing depth (Fig. 3). Sinkholes can occur due to failure of the overlying strata (Fig. 4). The collapsed material expands bell-shaped towards the depth. If soil is flushed away or backfill slipped away chimney caving can occur (Fig. 5).

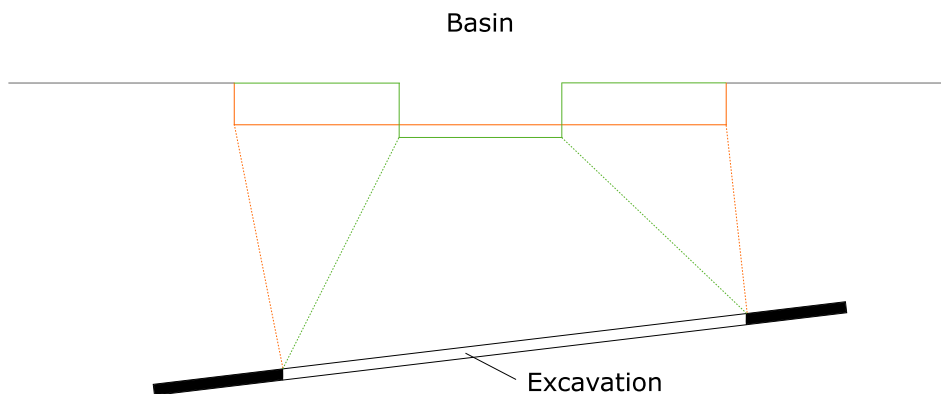


Fig. 1: Surface rupture – schematic representation

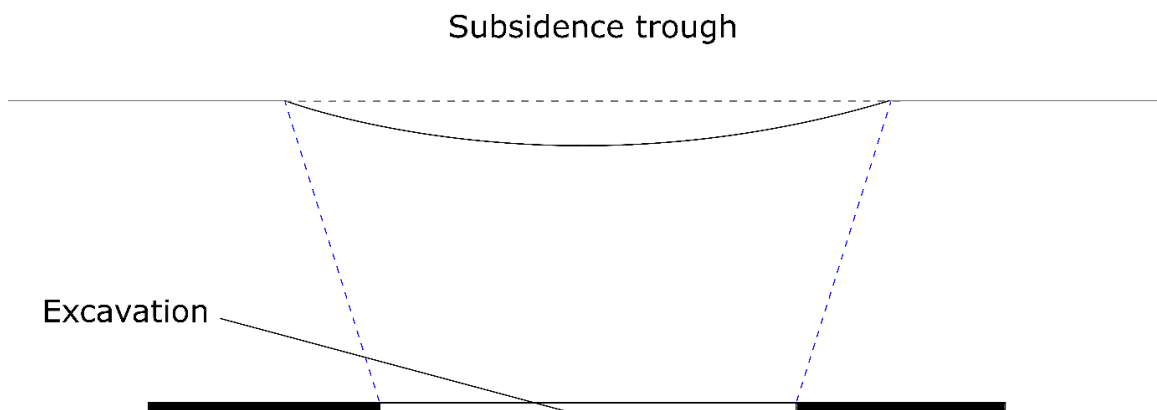


Fig. 2: Subsidence trough – schematic representation

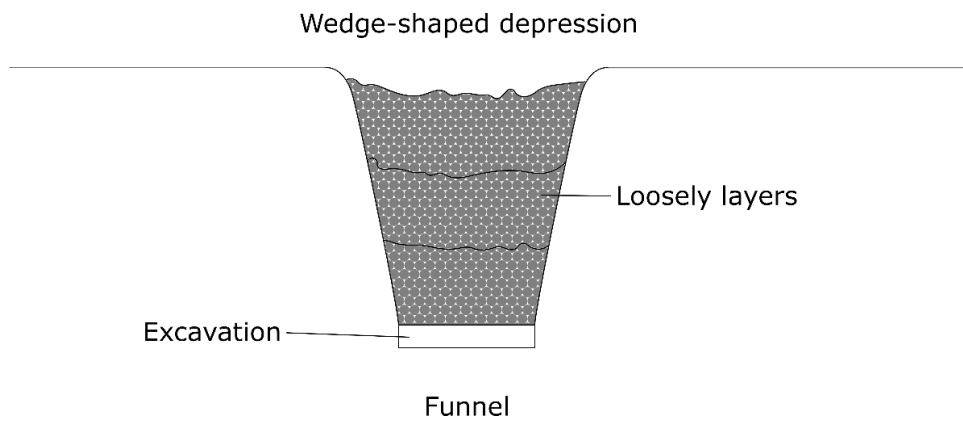


Fig. 3: Wedge-shaped depression – schematic representation (after Kratzsch, 1997)

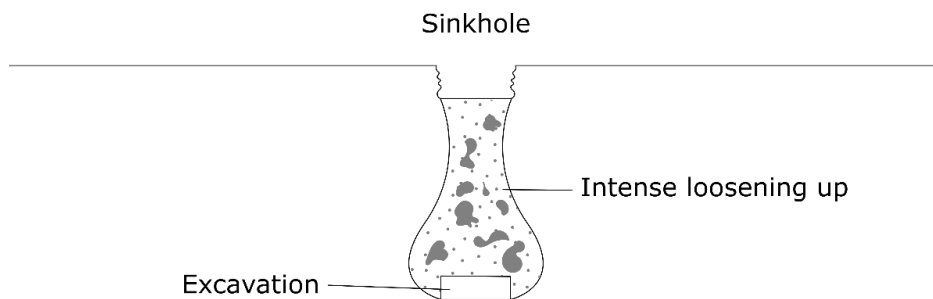


Fig. 4: Sinkhole – schematic representation (after Kratzsch, 1997)

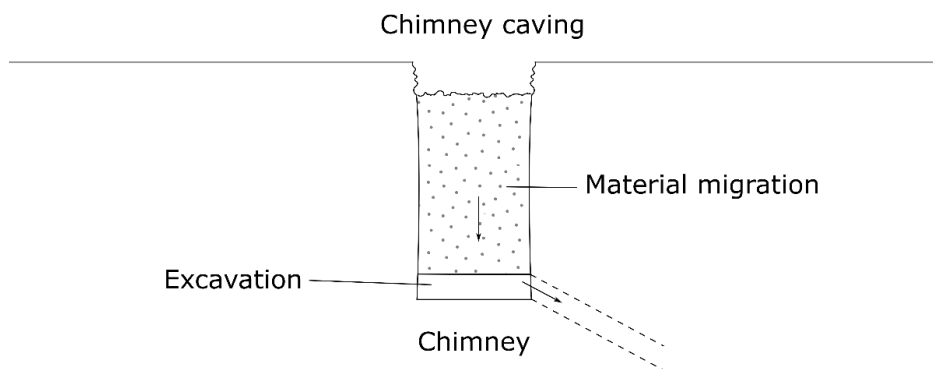


Fig. 5: Chimney caving – schematic representation (after Kratzsch, 1997)

Subsidence can be either continuous or discontinuous:

Continuous subsidence shows a smooth profile without jumps, steps or sudden profile changes. This type occurs at excavations of thin, horizontal or only slightly inclined deposits with soft and ductile sedimentary overburden. This is usually the case for longwall mining.

Discontinuous subsidence is characterized by large subsidence rates within a small area. Also, jumps, steps and sudden changes in the subsidence profile are typical. A common form of this type of subsidence are sinkholes connected with near-surface tunneling or karst-structures.

3 Continuous subsidence

The methods for calculation of subsidence can be classified as follows:

- empirical
- analytical
- numerical

Fundamentals

The general terms for a continuous subsidence trough are explained in Fig. 6. At point P the largest surface subsidence S_{max} is reached which increases with growing mining area. The methods explained below refer to the critical area of extraction and the critical angle ξ , which together with depth H of the mine determine the horizontal range of the subsidence effects. The critical angle ξ , and also the angle of draw ζ , describe the orientation of a connecting line between the boundary of the excavation area and that point at the surface where the subsidence reaches the value of zero. According to Kratzsch (1997) the maximum subsidence S_{max} is proportional to the thickness M of the excavation. In reality, the surface subsidence is always smaller than the thickness M of the excavation, since the lower strata experience tension, the immediate roof will be broken (caving) and the excavation will be filled with broken rock mass (loosening factor). This could be described by the following formula:

$$S_{max} = a \cdot M \quad (a < 1), \quad (3.1)$$

Where:

S_{max} ... Maximum surface subsidence

a Loosening factor

M Thickness of the excavation

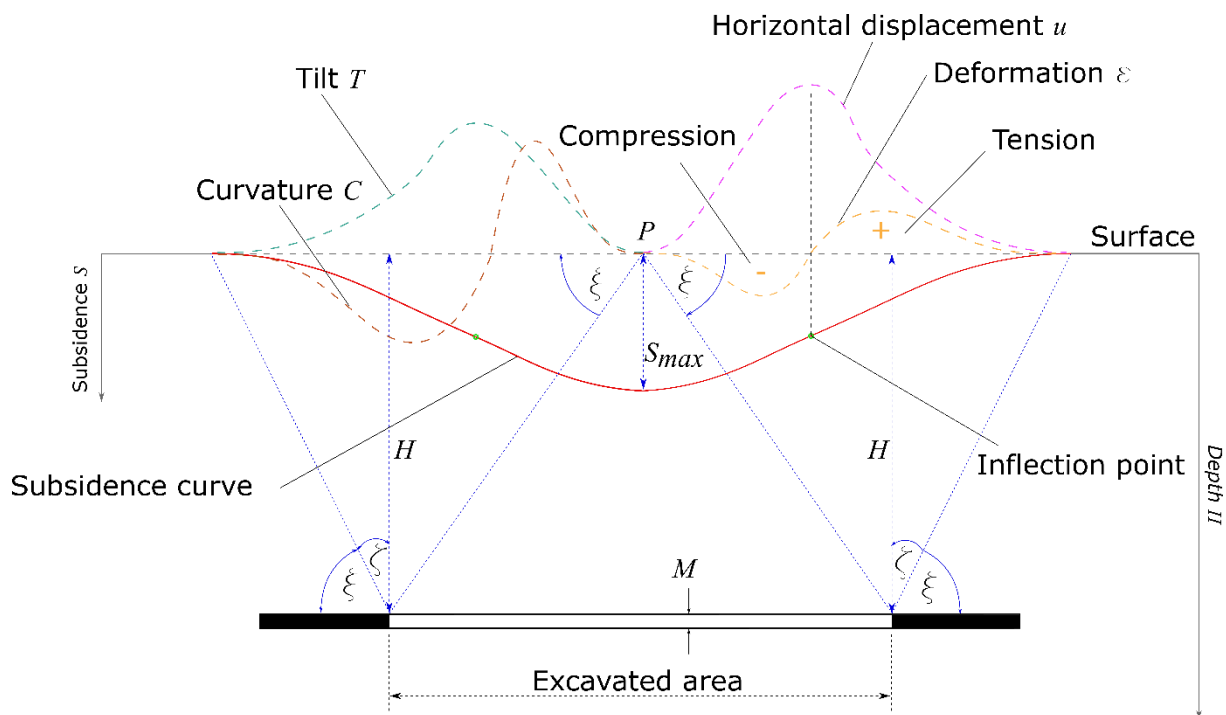


Fig. 6: Schematic representation of ground movement above an underground mine

The loosening factor a defines the proportion of the excavation thickness, which is measured as subsidence on the surface. This factor describes the loosening of the overburden rock layers. It is dependent on the mechanical properties of the rock mass, the mining layout and the type and quality of potential backfill. A general definition is given by the ratio between the volume of the subsidence trough V_M and the active subsidence volume V_A of the excavation:

$$a = \frac{V_M}{V_A}, \quad (3.2)$$

where:

a Loosening factor

V_M ... Volume of the subsidence trough

V_A ... Active subsidence volume

The factor a applies only to critical and supercritical states. If the full subsidence level S has not yet been reached (subcritical state), the loosening factor a is called apparent loosening factor a_{ap} (Peng, 2008):

$$S = a_{ap} \cdot M \quad (a < 1), \quad (3.3)$$

where:

S Surface subsidence

a_{ap} ... Apparent loosening factor

M Thickness of the excavation

Typical empirical values for the loosening factor a are given in Tab. 1. If the same area is excavated at larger depth, the critical angle γ increases. The subsidence trough becomes wider but less deep. For this case, an additional parameter must be used, the exposure factor e (Kratzsch, 1997). The following formula is given for the maximum subsidence S_{max} :

$$S_{max} = e \cdot a \cdot M, \quad (3.4)$$

where:

S_{max} ... Maximum subsidence

e Exposure factor

M Thickness of the excavation

Tab. 1: Empirical values for loosening factor a

Type of mining	Loosening factor a
Caving	0.90 – 0.99
Backfill	0.50 – 0.90
Yielding pillars	0.30 – 0.60

The exposure factor e is also an empirical value and must be adapted to the respective rock mass conditions.

Horizontal displacements u are directed towards the excavation face and have a symmetrical shape in general. The following relation is valid for the maximum displacement u_{\max} :

$$u_{\max} = 0.4 \cdot S_{\max} \quad (3.5)$$

where:

u_{\max} ... Maximum horizontal displacement

This maximum lies in the region at the inflection point of the subsidence profile and near the excavation faces. The deformation ε along the subsidence trough depends on the elongation of adjacent points. If the elongation is positive, tensile strain and stresses will be produced and vice versa. The transition between tension and compression is defined by the inflection point.

First derivation with respect to location x of the subsidence curve gives the tilt. Second derivation with respect to location x gives the curvature:

$$\begin{aligned} T(x) &= S(x) \cdot \frac{d}{dx} \\ C(x) &= S(x) \cdot \frac{d^2}{dx^2} \end{aligned} \quad (3.6)$$

The maximum tilt is situated at the inflection points of the subsidence profile. A geometrical calculation of tilt and geometrical approximation of curvature is the following:

$$\begin{aligned} T_{i,i+1} &= \frac{S_{i+1} - S_i}{l} \\ C_i &\approx \frac{S_{i+1} - 2 \cdot S_i + S_{i-1}}{l^2} \end{aligned} \quad (3.7)$$

In addition to these calculations, Fig. 7 shows the location of the measurement points.

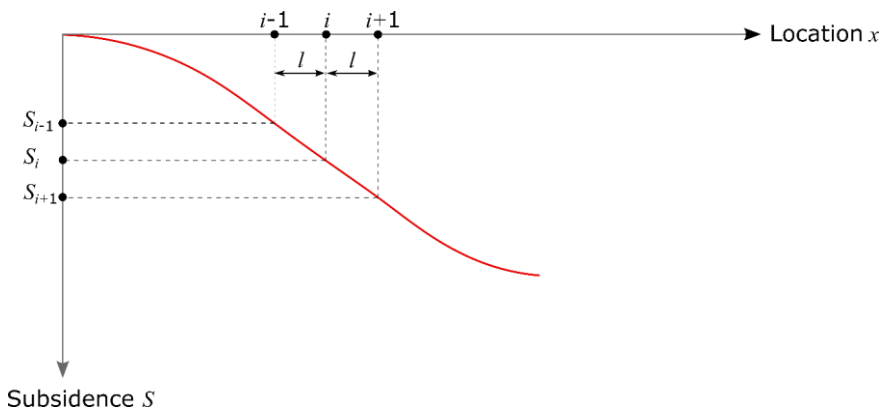


Fig. 7: Location of measurement points for determination of tilt and curvature

Dynamic ground movements are declared by subsidence velocity \dot{S} , subsidence acceleration \ddot{S} and deformation velocity $\dot{\varepsilon}$. These values are the first and second derivative with respect to time of subsidence and deformation:

$$\begin{aligned}\dot{S} &= S(x,t) \cdot \frac{d}{dt} \\ \ddot{S} &= S(x,t) \cdot \frac{d^2}{dt^2}, \\ \dot{\varepsilon} &= \varepsilon(x,t) \cdot \frac{d}{dt}\end{aligned}\quad (3.8)$$

where:

\dot{S} Subsidence velocity,
 \ddot{S} Subsidence acceleration,
 $\dot{\varepsilon}$ Deformation velocity,
 $S(x,t)$... Subsidence function in time and space,
 $\varepsilon(x,t)$... Deformation function in time and space.

Fig. 8 illustrates the face advance of an underground excavation. The face advance is subdivided into three stages to show the development of the subsidence (National Coal Board, 1975). The excavation is slightly oblique and thus characterized by an increase in mining depth from H_1 to H_4 . The subsidence trough for the subcritical state is given by the green line. The maximum subsidence S_{\max} is reached for the critical state (red line). Areas beyond this range are called supercritical (magenta line). Here, the subsidence has already reached its maximum and shows only further extension in the horizontal direction.

The critical width w_c (critical range) is calculated as follows (National Coal Board, 1975):

$$w_c = 2 \cdot H \cdot \tan \zeta \quad (3.9)$$

where:

w_c ... Critical width
 H ... Depth of the excavation
 ζ ... Angle of draw

Another equation for the critical width w_c (critical state) for underground coal mines is (Luo & Peng, 1997):

$$w_c = 100 + 1.048 \cdot H \quad (3.10)$$

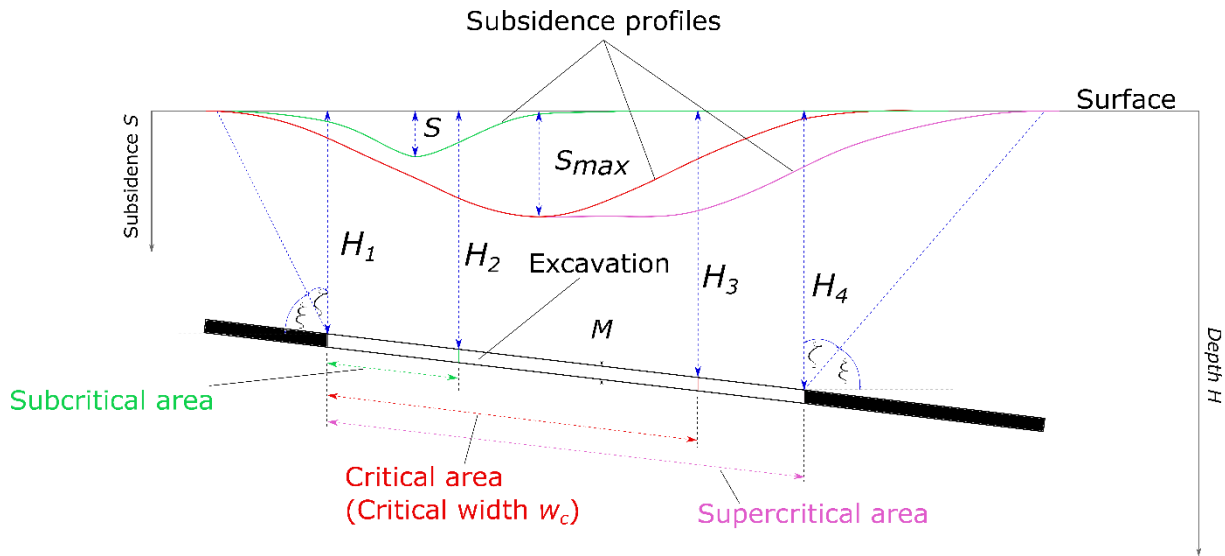


Fig. 8: Schematic representation of subsidence evolution with face advance

If the location of vanishing surface subsidence and S_{max} are known, the subsidence profile can be calculated by the using influence or profile functions.

The time delay between the excavation volume and the development of a subsidence trough will be considered by the time coefficient tc (Zimmermann, 2011):

$$tc = \frac{1}{\Delta t} \tag{3.11}$$

where:

Δt ... time delay

Profile functions

Profile functions (Fig. 9) are used to describe the shape of subsidence trough. They have the following general form:

$$S = S_{max} \cdot f(B, x, C) \tag{3.12}$$

where:

S_{max} ... Maximum subsidence

B Critical radius

x Horizontal distance to auxiliary points

C Constant or additional function (depending on type of mining, geology, etc.)

The critical radius is calculated as follows:

$$\begin{aligned} B &= H \cdot \tan(\zeta) \\ B &= H \cdot \cot(\xi) \end{aligned} \tag{3.13}$$

where:

H ... Mining depth

ζ ... Angle of draw

ξ ... Critical angle

Exponential, trigonometric, hyperbolic or error functions are used to describe the subsidence trough. The method with a negative exponential function finds application in considering subcritical states due to the asymmetric behaviour around the inflection point (Peng & Cheng, 1981):

$$S(x) = S_{\max} \cdot e^{-m \left(\frac{x}{w_s} \right)^n} \quad (3.14)$$

where:

S Subsidence

x Distance to the centre of the subsidence trough

w_s Half width of the subsidence trough

m, n ... Empirical coefficients

The half width w_s of the subsidence trough is determined by (after Peng, 2008):

$$w_s = \frac{w}{2} + B \quad (3.15)$$

where:

w_s Half width of the subsidence trough

w Width of the excavation

B Critical radius

According to Brady & Brown (2004) the approach with a hyperbolic function (Peng & Cheng, 1981) provides the best results:

$$S(x) = \frac{1}{2} \cdot S_{\max} \left[1 - \tanh \left(\frac{b \cdot x}{H} \right) \right] \quad (3.16)$$

The empirical coefficient b is determined on the basis of the experience for a specific mining area. Hyperbolic functions are more suitable for critical and supercritical states because of their symmetry around the inflection point. Another hyperbolic function is proposed by Karmis, Goodman & Hasenfus (1984):

$$S(x) = \frac{1}{2} \cdot S_{\max} \left[1 - \tanh \left(\frac{b \cdot x}{w_i} \right) \right] \quad (3.17)$$

where:

x Distance to the inflection point of the subsidence trough

w_i Distance between centre and inflection point of the subsidence trough

Profile functions are easy to apply, but they are valid only for the considered region. Parameters of the excavation, geology of the overburden and depth of the mine have significant influence.

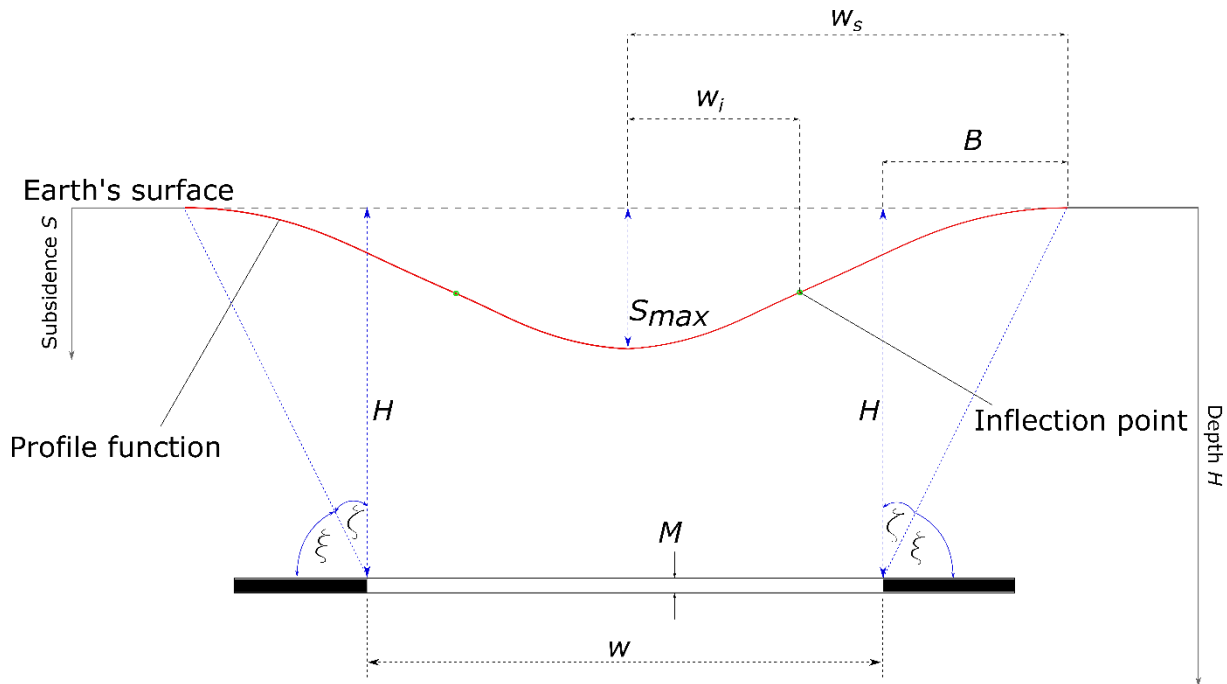


Fig. 9: Schematic illustration of a profile function with parameters

Influence functions

Influence functions are used to describe the impact of the smallest excavation areas to the earth's surface. According to the principle of superposition, the subsidence profile for the complete excavation can be determined by integrating the influence function $p(r)$ over the excavation area. The use of a numerical integration provides subsidence predictions for mining areas of any shape.

The influence function $p(r)$ yields the influence of subsidence at a point P of the earth's surface depending on a small element dA at a point P' in the underground as a function of r (horizontal projection of P to P') as shown in Fig. 10. P has the coordinates x, y (plane on the earth's surface) and P' has the coordinates ζ and η . This plane is shown in Fig. 11. This results in the following form for the influence function $p(r)$ (Brady & Brown, 2004):

$$p(r) = \omega(\zeta, \eta) \cdot f(r) \tag{3.18}$$

where:

p Influence value

$\omega(\zeta, \eta)$... Weighting factor (consideration of variations in mining height M)

r Horizontal distance from P to P'

The horizontal distance r is calculated as:

$$r = \sqrt{(x - \zeta)^2 + (y - \eta)^2} \tag{3.19}$$

where:

x, y Coordinates of P

ζ, η ... Coordinates of P'

The subsidence S of a region A can be determined with $dA = d\zeta \cdot d\eta$ by integration (Brady & Brown, 2004):

$$S(x, y) = \int_{\eta} \int_{\zeta} \omega(\zeta, \eta) \cdot f\left(\sqrt{(x - \zeta)^2 + (y - \eta)^2}\right) d\zeta d\eta \quad (3.20)$$

In Germany and Eastern Europe, trigonometric or exponential functions of the following form are used (Brauner, 1973):

$$p(r) = k_1 \cdot S_c \cdot f(B, r, k_2) \quad (3.21)$$

where:

p Influence value

k_1 Constant

B Critical radius

r Horizontal distance from P to P'

k_2 Constant

A widespread function is (Brady & Brown, 2004):

$$p(r) = \frac{n \cdot S_{max}}{B^2} \cdot e^{-n \cdot \pi \cdot \left(\frac{r}{B}\right)^2} \quad (3.22)$$

With the parameter n which characterise the properties of the rock mass

By integration over large areas, it may be possible that obtained influence functions coincide with the profile functions because they are mathematically unambiguous. Profile functions have the advantage to be easily obtained. However, influencing functions are more adaptable to the posed problem and they are more suitable for geometrically irregular mining areas.

In case of several panels, the superposition principle can be applied for the construction of the final subsidence trough like shown in Fig. 11. It should be noticed, that above outlined calculation procedures were widely used for a long time, but they have one general major disadvantage: they are pure geometrical with some empirical functions considering rock mass behaviour and do not incorporate the behaviour of the rock mass in a physical manner. Therefore, due to the progress in numerical simulation methods, these techniques are more and more replaced by predictions based on numerical calculations using constitutive models to describe the rock mass behaviour.

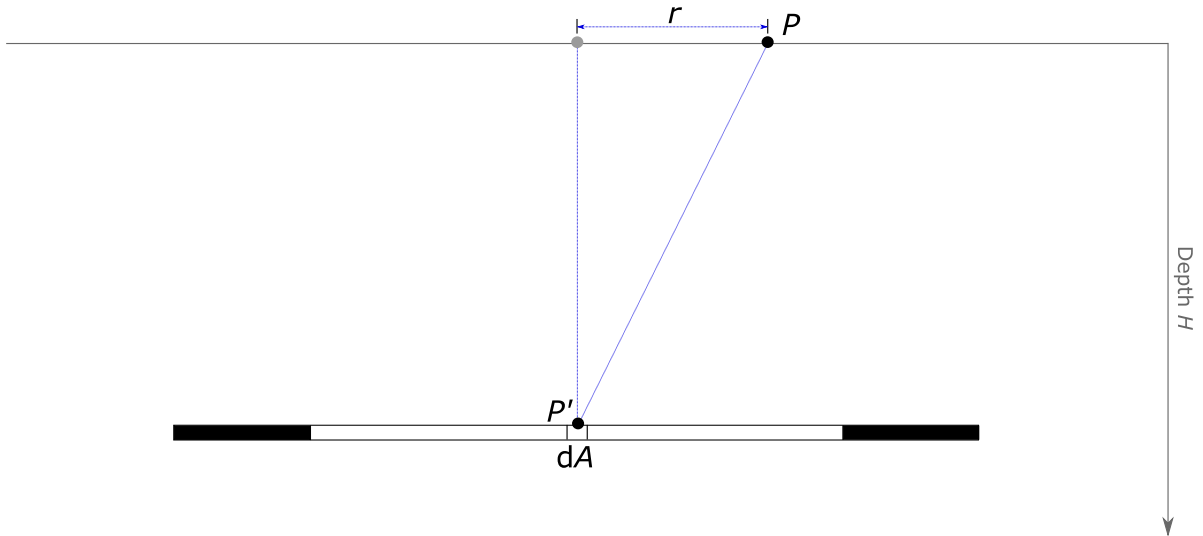


Fig. 10: Extracted element of the mining area (after Brady & Brown, 2004)

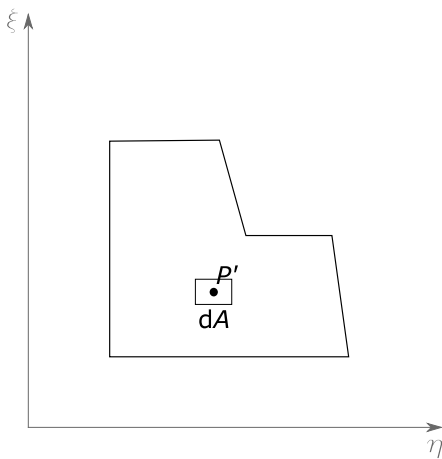


Fig. 11: Excavation with extracted element (after Brady & Brown, 2004)

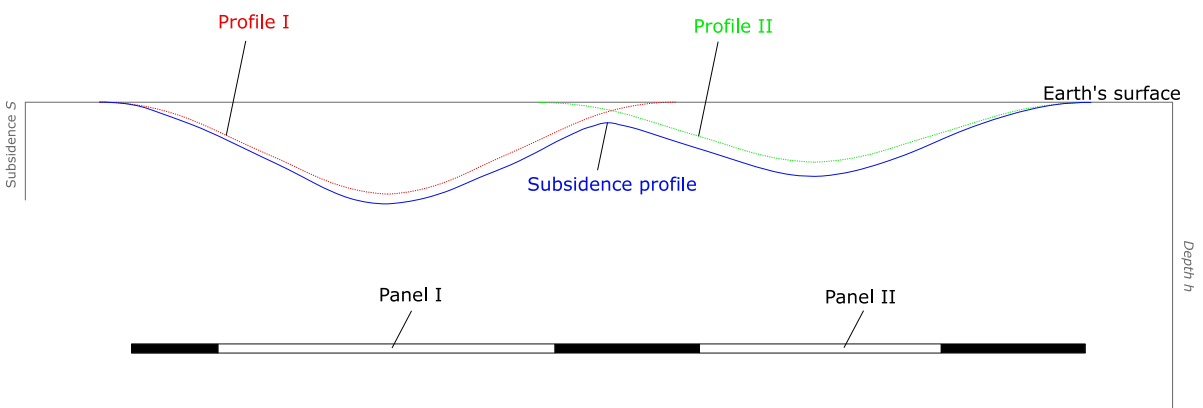


Fig. 12: Resulting subsidence profile of adjacent mining panels

4 Influence of geological effects and mining parameters

In the case of mining, shape and size of the subsidence trough is depending on the mining method, the depth and the rock mass conditions. All points inside the subsidence area except the center are influenced by horizontal and vertical movements. The center is subjected only to vertical movement. The shape of the subsidence basin depends on the geometry and the dip angle of the excavation. If the excavation is horizontal with a rectangular base, the shape of the subsidence profile is elliptical. Factors influencing the subsidence profile are shown in Tab. 2.

Tab. 2: Influencing factors of the subsidence profile (Peng, 2008)

Influencing factor		Effect
Properties of the overburden	Hard and strong	Subsidence is lower
	Soft and weak	Subsidence is higher
Angle of dip of the excavation	Horizontal to slightly dipping	Surface movement direction mainly vertical
	Steeply dipping	Surface movement direction parallel and vertical
Excavation	High	Size of the geosyncline increases
		Subsidence profile becomes weaker and deformations decrease (deformations are inversely proportional to the mining depth)
		Velocity of surface movements decreases (velocity of maximum surface movements is inversely proportional to mining depth)
	Low	Temporal duration of surface movements increases
		Subsidence profile is stronger pronounced and deformations increase
		Velocity of surface movements increases
Ratio of excavation depth to mining thickness	$\frac{H}{M}$ is increasing	Deformations decrease and are less pronounced
	$\frac{H}{M}$ is very small	Large cracks on the earth's surface, steps or sinkholes can arise
Size of excavation	Increasing	Subsidence increases
	Decreasing	Subsidence decreases
	Development coefficients to determine the degree of subsidence	$n_1 < 1$ or $n_2 < 1$: Shape of the excavation is subcritical and surface movements have not reached the full extent

	$n_1 = C \cdot \frac{L}{H} \text{ und } n_2 = C \cdot \frac{W}{H}$ <p>where: Crock property influence coefficient L, W ... Length, width of excavation H ... Mining depth</p>	$n_1 > 1$ and $n_2 > 1$: Excavation is in the critical or over-critical range and surface movements are fully developed
Multiple-panel mining in horizontal or vertical direction	The subsidence profile of adjacent excavations depends on the geological situation, the geometry, the mining depth as well as the mining height	Differences in these properties lead to a differentiated expression of the final subsidence profile Subsidence profiles can overlap (Fig. 12)
Faults / discontinuities	Angle of dip, size, strength, position	Could lead to increased shear displacements in the area of the fault and weakness zones as well as to cracks or steps on the earth's surface Intensity depends on these parameters
Topography	Steep slopes in the area of the geosyncline	Stability can be adversely affected and it can lead to landslides
	Topographic height	Gentry (1977) showed that subsidence is higher at the highest topographic points than at the lowest topographic points

5 Discontinuous subsidence

In case of mining close to the surface, sinkholes (Fig. 13) can occur during or after the excavation. Sinkholes are connected with a mass deficit. The original cavity is partially filled (partial collapse) and later possibly completely filled (full collapse) by rock mass or soil under gravitational load. The sinkhole develops from the excavation upwards until it reaches the surface.

Empirical models

The hazard assessment is based on statistical analyses of observed sinkholes. Geological, hydrogeological and geomechanical factors are considered. In most cases, only rough statements are possible and a strong regional distinction has to be taken into account. The following empirical models are widespread in Germany.

Fenk (1981) developed empirical rules to predict:

- Relative fracture probability
- Time-to-failure
- Final diameter of sinkhole
- Horizontal distance from excavation face to the sinkhole edge

Fenk (1979, 1981, 1984 and 1994) includes the following factors:

- Mining and rock mass parameters
 - Dimension of excavation
 - Form of excavation
 - Support and backfill of excavation
 - Depth of excavation
 - Excavation height
 - Dip angle of deposit
 - Rock and rock-matrix properties of the overlying strata
 - Groundwater level above the excavation
 - Water supply of the excavation
- Morphology and usage of the Earth's surface
- Climate and rainfall

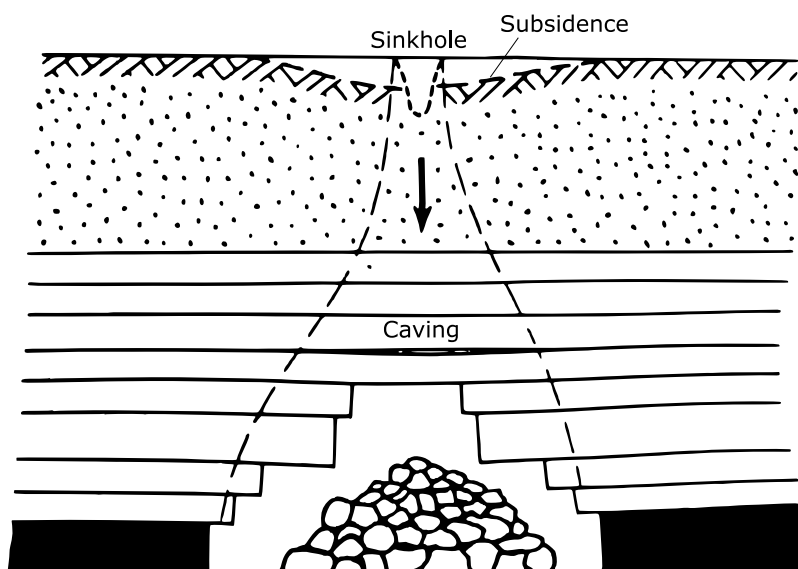


Fig. 13: Funnel-shaped sinkhole caused from cave-in of rock material (Kratzsch, 1997)

- Subrosion and suffocation in the overburden
- Traffic

Lerche & Lempp (2002) evaluated openings according to different aspects by the help of data analysis and classification schemes. Based on these data it is possible to predict the occurrence of sinkholes. This procedure is not restricted to man-made excavations, but applicable to all types of caves.

Analytical models

5.1.1 Volume balance models

Predictions for sinkhole hazards is made by comparing (balancing) the volume of the cavity with the volume of broken rock mass for an assumed growth of the cavity. This is defined by a loosening factor fl :

$$fl = \frac{V_A}{V_B} \quad (5.1)$$

with:

fl Loosening factor (> 1)

V_A Volume of broken mass

V_B Volume of intact rock mass

The value of the loosening factor depends on the rock mass type and the stability of the loosened material. Typical values are shown in Tab. 3. Thus, a distinction can be made between temporary loosening factor and final (long-term) loosening factor. (Reuter & Waldmann, 1978; Penzel, 1981)

Eckart (1973) provides an estimate for the limit of rock thickness H_{max} . If the depth of the excavation is lower than H_{max} , there is no risk for a sinkhole.

$$H_{max} = \frac{0.0127 \cdot (100 - bf) \cdot M}{fl - 1} \quad (5.2)$$

Tab. 3: Typical loosening factors

Rock mass type	Loosening factor fl
Loess	1.2
Clay	1.2 – 1.5
Sand	1.2 – 1.4
Lignite	1.2
Limestone	1.6 – 1.9
Sandstone	1.6 – 2.0
Shale	1.4 – 1.5
Palaeozoic shale	1.7

where:

bf Backfill (%)

M Mining height

However, is the cavity located at the same level or higher than H_{\max} , an additional check for sinkhole risk must be carried out. The boundary conditions of this method are: (1.) no horizontal material transports of the loosened rock masses and (2.) the fractured (loosened) rock mass above the cavity has the shape of a half-ellipse (Eckart, 1972).

Meier (1978 and 2001) put together analytical solutions for the volume balance between broken rock mass and open space (cavity) for several geometrical constellations (Fig. 14 to Fig. 17):

- a) Sinkhole is bordered by vertical fracture planes over a lateral delimited cavity (gallery, drift etc.)

$$H_{\max} = \frac{M}{fl-1} \cdot \left(1 + \frac{M}{l \cdot \tan \phi} \right) \quad (5.3)$$

where:

M Opening height

ϕ Dumping angle

- b) Sinkhole (vertical half-ellipse) over the laterally delimited cavity (gallery, drift, load mining, etc.)

$$H_{\max} = \frac{1,274 \cdot M}{fl-1} \cdot \left(1 + \frac{M}{l \cdot \tan \phi} \right) \quad (5.4)$$

with the angle of repose ϕ .

- c) Chimney-like sinkhole with vertical fracture planes above cave without lateral boundaries for mass flow

$$H_{\max} = \frac{M}{fl-1} \cdot \left(1 + \frac{M}{\frac{l}{2} \cdot \tan \phi} + \frac{M^2}{\frac{3}{2} \cdot l^2 \cdot \tan^2 \phi} \right) \quad (5.5)$$

with:

ϕ Angle of repose

l Width of chimney

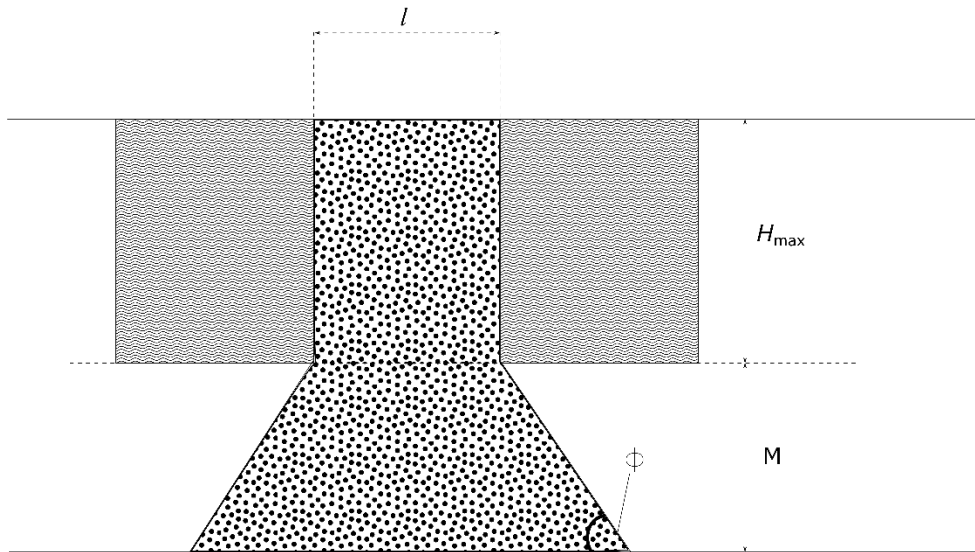


Fig. 14: Schematic illustration of a sinkhole with vertical boundaries above a laterally delimited excavation

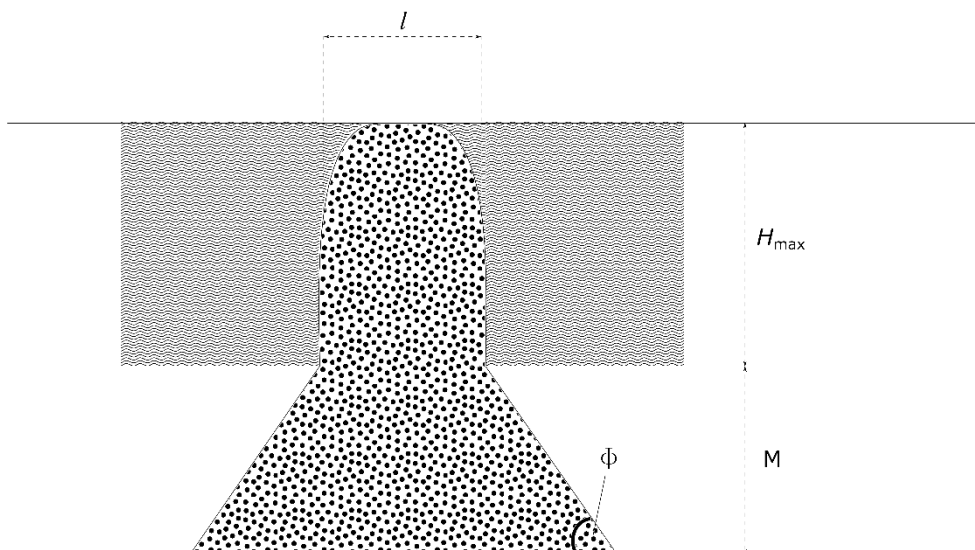


Fig. 15: Schematic illustration of a sinkhole of half-elliptical shape above a laterally delimited excavation

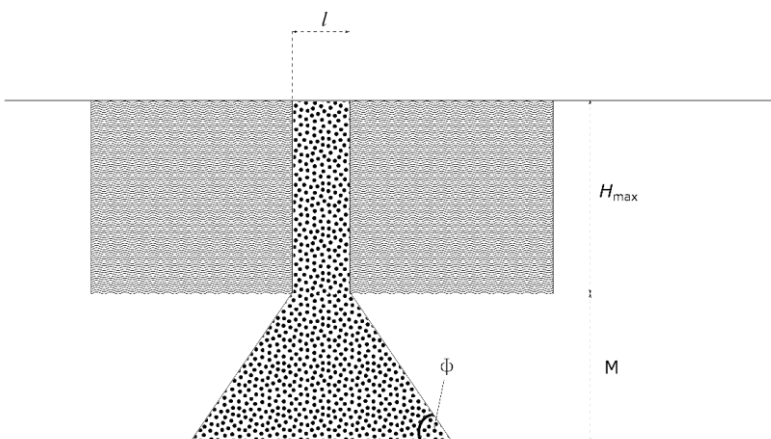


Fig. 16: Schematic illustration of a sinkhole as vertical chimney above an excavation

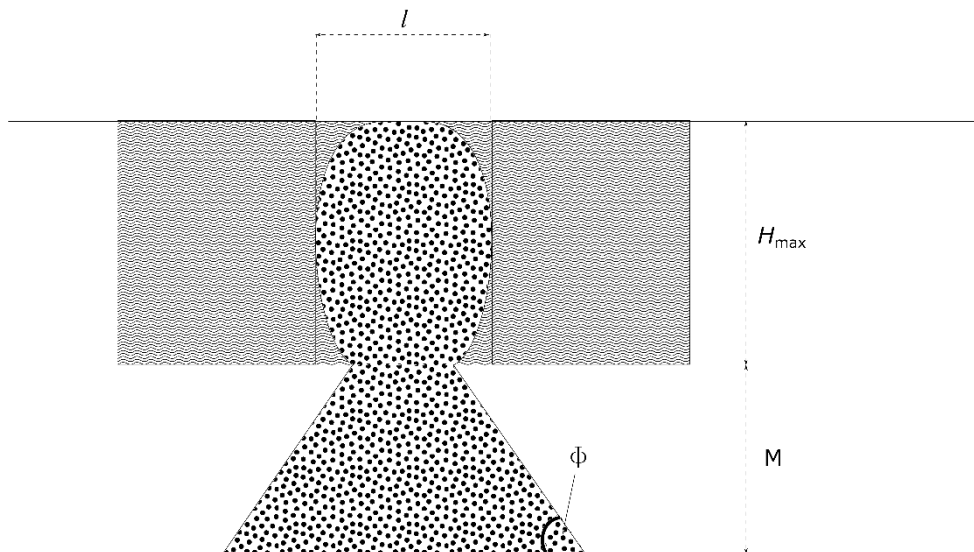


Fig. 17: Schematic illustration of spheroidal fracture above an excavation

- d) Sinkhole (spheroid) above an excavation without lateral boundaries for the collapsed masses

$$H_{\max} = \frac{3}{2} \cdot \frac{M}{fl-1} \cdot \left(1 + \frac{M}{\frac{l}{2} \cdot \tan \phi} + \frac{M^2}{\frac{3}{2} \cdot l^2 \cdot \tan^2 \phi} \right) \quad (5.6)$$

with:

ϕ Angle of repose

l Maximum width of sinkhole

Drift intersections are often the most critical locations for the evolution of sinkholes. According to Meier & Meier (2005) and Clostermann et al. (2020) H_{\max} can be estimated according the following formula:

$$H_{\max} = \frac{4M}{\pi b(fl-1)} \cdot (2M \cdot \cot(\phi) + 1.8b) \quad (5.7)$$

with:

b width of drifts forming the intersection

5.1.2 Simple geomechanical models

Over the years a lot of geomechanical models based on force or stress equilibrium have been proposed. A few of them are presented below.

a) Model Liszkowski

Based on Terzaghi (1943) and Protodjakonov (1926), Liszkowski (1973) assumed that an arch-shaped damage area of height H_{Br} forms above the opening:

$$H_{Br} = \frac{\frac{w}{2} + M \cdot \tan\left(45^\circ + \frac{\theta}{2}\right)}{k} \quad (5.8)$$

with:

H_{Br} Height of the arch-shaped damage area

w Width of opening

M Opening height

θ Internal friction angle

k Strength coefficient after Protodjakonov

The strength coefficient k after Protodjakonov (1926) is a general indicator of rock mass resistance and can be defined as follows:

$$k = \frac{\sigma_c}{10} \quad (5.9)$$

where σ_c is the uniaxial compressive strength. Based on this coefficient, Protodjakonov (1926) divided rock mass into 15 categories as shown in Tab. 4.

Tab. 4: Classification of the rock mass (after Protodjakonov, 1926)

Category		Rock mass types	Strength coefficient k
I	High strength	Compact quartzite, basalt	20
II	Very strength	Rhyolite, very hard granite rocks, compact granites, schist quartzite, strong sandstones and limestones, flint shales	15
III	Regular strength	Granites (rubble), very compact limestones and sandstones, iron ore, conglomerates	10
III-a	Regular strength	Dolomites, compact limestones and sandstones, marbles	8
IV	Fairly strength	Cracked quartzite, ordinary sandstones	6
IV-a	Fairly strength	Sandstone clay schist, schist sandstone	5

V	Moderate strength	Schist, weak sandstones and limestones, soft conglomerates	4
V-a	Moderate strength	Weaker schist, marl, weaker iron ore	3
VI	Fairly soft	Soft schist, very soft limestone, cracked sandstone, chalk, halite, gypsum, frozen ground, coal, marl	2.2
VI-a	Fairly soft	Decomposed schist, strength coal, hardened clay, wet soft iron ore	1.5
VII	Soft	Compressed clay, coal with medium strength, clayey soil	1
VII-a	Soft	Loess, soft coal	0.8
VIII	Soil	Agriculture soil, peat, wet sand	0.6
IX	Mould	Sand, fine grained gravel, heaps	0.5
X	Liquid	Quicksand, muddy soil, highly wet soil	0.3

H'' defines the lower limit for the tensile stress zone according to Therzaghi (1943):

$$H'' = \frac{5}{2} \cdot \frac{c}{\rho \cdot g} \cdot \tan\left(45^\circ + \frac{\theta}{2}\right) \quad (5.10)$$

where:

H'' Lower limit of tensile stress zone

c Cohesion

ρ Density

g Gravity

θ Internal friction angle

If the damaged zone reaches or exceeds this limit a sinkhole is formed.

b) Model Jarosz

Jarosz (1975) considered clay and sand layers of thickness H'' , assuming that a vertical chimney-shaped cave develops if the arch-shaped damage area with height H_{Br} reaches these layers (Fig. 18). The distance from the roof of the excavation to the lower boundary of the tensile stress zone is represented by the thickness H' . A sinkhole is predicted if $H' < H_{Br}$. The height H_{Br} of the arch-shaped damage area is calculated as follows:

$$H_{Br} = \frac{w}{2} \cdot \left(\frac{1}{v} - 1\right) - \frac{M}{2} \quad (5.11)$$

where:

H_{Br} Height of the arch-shaped damage area

w Width of opening
 M Opening height
 ν Poisson's ratio

c) Model Penzel

Penzel (1980) assumes an axially symmetric cylindrical failure body and balances the tangential forces (driving force vs. frictional resistance). It is assumed that the overburden layers are homogeneous. Loosening of the rock mass is not considered. The thickness threshold H_{\max} is calculated as follows:

$$H_{\max} = \frac{\frac{w}{2} - 2 \cdot \frac{c}{\rho \cdot g}}{\tan(\theta) \cdot \lambda} \quad (5.12)$$

where:

H_{\max} ... Threshold thickness of rock mass
 c Cohesion of rock mass
 ρ Density of rock mass
 g Gravity
 θ Internal friction angle
 λ Coefficient of lateral earth pressure

d) Model Bierbaumer

Bierbaumer (1913) assumed vertical sliding faces above the excavation up to the earth's surface (Fig. 19) and considered the equilibrium along these sliding faces:

$$Q - 2 \cdot T = P \quad (5.13)$$

where:

Q ... Weight force of the sliding mass
 T ... Tangential forces by friction on sliding faces
 P ... Support load

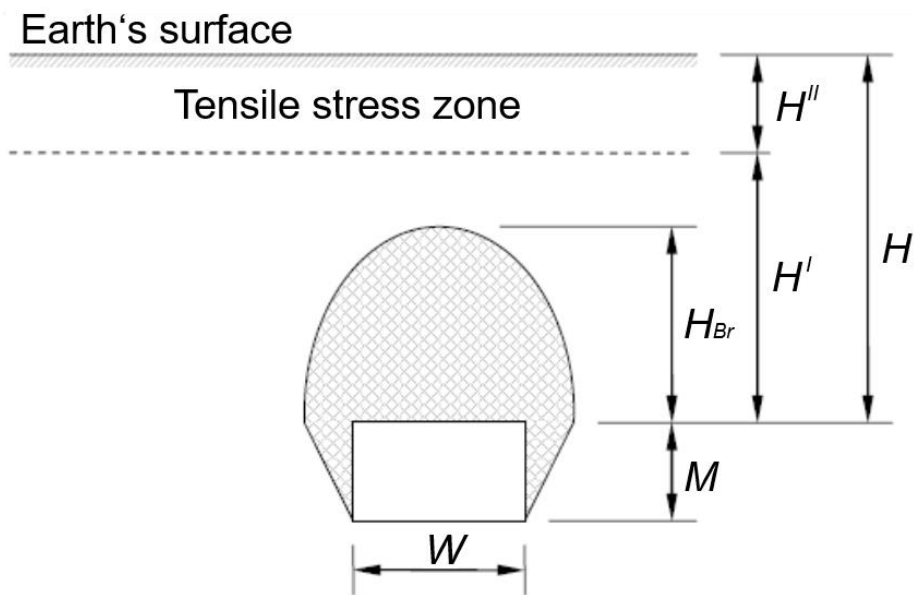


Fig. 18: Arch shaped damage model

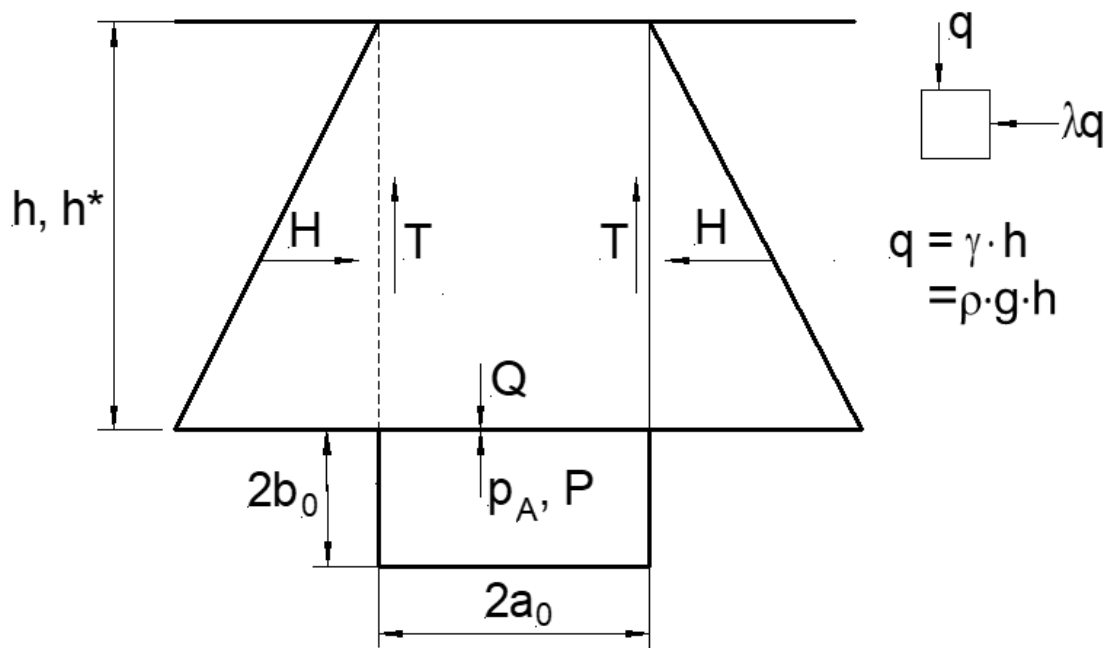


Fig. 19: Model with vertical sliding faces above the excavation

The individual components of this equilibrium are:

$$\begin{aligned}
 Q &= 2 \cdot a_0 \cdot \rho \cdot g \cdot h \\
 T &= H \cdot \tan(\phi) \\
 H &= \frac{h}{2} \cdot \lambda \cdot q = \frac{1}{2} \cdot \lambda \cdot \rho \cdot g \cdot h^2
 \end{aligned}
 \tag{5.14}$$

where:

- Q Weight force of the sliding mass
- T Tangential forces by friction on sliding faces
- P Support load
- $2a_0$ Width of the excavation
- ρ Density
- g Gravity
- h Height of the overburden
- H Lateral forces
- ϕ Friction angle
- λ Coefficient of lateral pressure

Substituting these terms into the equation of equilibrium, gives support load P :

$$P = a_0 \cdot \rho \cdot g \cdot h \cdot \left(2 - \lambda \cdot \frac{h}{a_0} \cdot \tan(\phi) \right)
 \tag{5.15}$$

$$P_A = \frac{P}{2 \cdot a_0}
 \tag{5.16}$$

where:

- P Support load
- P_A Active support pressure

e) Model Salustowicz

Salustowicz (2009) supposed that the weakness area do not reach the earth's surface. The height h^* of the failed area is smaller than the height h considered by Bierbaumer. The support load P becomes than a function of height h :

$$P = P(h)
 \tag{5.17}$$

Extreme values for this function are:

$$\begin{aligned}
 0 &= \frac{dP}{dh} \\
 0 &= 2 \cdot a_0 \cdot \rho \cdot g - 2 \cdot \lambda \cdot \rho \cdot g \cdot h \cdot \tan(\phi) \\
 0 &= 2 - 2 \cdot h \cdot \frac{\lambda \cdot \tan(\phi)}{a_0} \\
 h &= \frac{a_0}{\lambda \cdot \tan(\phi)} \\
 \rightarrow h &= h^*
 \end{aligned} \tag{5.18}$$

The support load P for the height h^* is calculated as follows:

$$\begin{aligned}
 P(h^*) &= a_0 \cdot \rho \cdot g \cdot h^* \cdot \left(2 - \lambda \cdot \frac{h^*}{a_0} \cdot \tan(\phi) \right) \\
 &= a_0 \cdot \rho \cdot g \cdot \frac{a_0}{\lambda \cdot \tan(\phi)} \cdot \left(2 - \lambda \cdot \frac{\frac{a_0}{\lambda \cdot \tan(\phi)}}{a_0} \cdot \tan(\phi) \right) \\
 &= \frac{a_0^2 \cdot \rho \cdot g}{\lambda \cdot \tan(\phi)}
 \end{aligned} \tag{5.19}$$

Fig. 20 shows the behaviour of the support load for increasing depth for the two theories after Bierbaumer and Salustowicz.

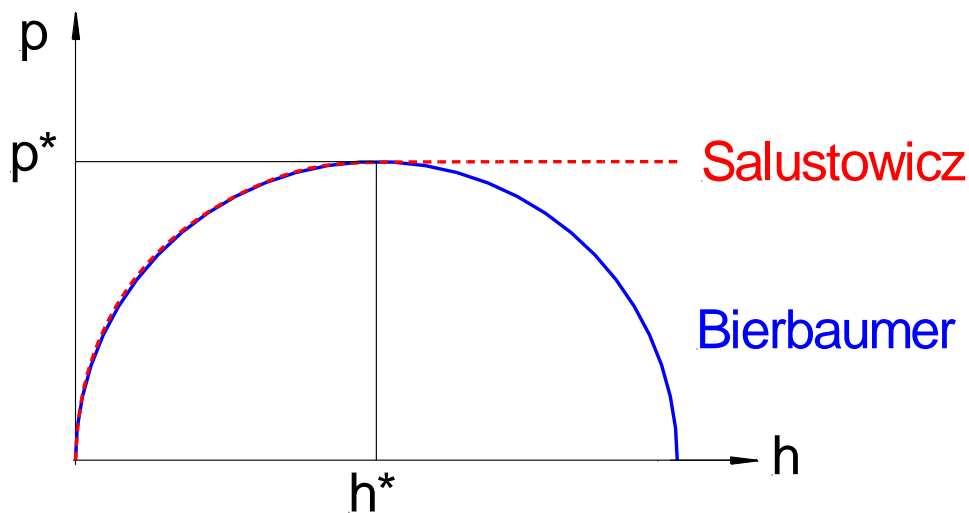


Fig. 20: Comparison of the theories of Bierbaumer and Salustowicz

f) Model Terzaghi

Terzaghi assumed a failed area above an excavation with lateral borders by sliding faces (Fig. 21). His approach is based on differential equilibrium (equilibrium at infinitesimal small strips) considering the Mohr-Coulomb criterion.

The primary state of stress is given by:

$$\begin{aligned}\sigma_r &= \rho \cdot g \cdot z = \sigma_z(z) \\ \sigma_n &= \rho \cdot g \cdot z = \sigma_h(z)\end{aligned}\quad (5.20)$$

where:

σ_r, σ_z Stress in vertical direction
 σ_n, σ_h Stress in horizontal direction
 ρ Density
 g Gravity
 z Depth

The Mohr-Coulomb failure criterion is given by:

$$\tau = \sigma_h \cdot \tan(\phi) + C \quad (5.21)$$

where:

τ Shear stress
 σ_h Stress in horizontal direction (normal stress)
 ϕ Friction angle
 C Cohesion

The self-weight of the considered strip is:

$$dG = \rho \cdot g \cdot 2 \cdot a_0 \cdot dz \quad (5.22)$$

where $2a_0$ is the width of the excavation.

The force equilibrium in the vertical direction (z-direction) is given by:

$$\begin{aligned}2 \cdot a_0 \cdot \sigma_r + dG - 2 \cdot a_0 \cdot (\sigma_r + d\sigma_r) - 2 \cdot \tau \cdot dz &= 0 \\ \sigma_v &= \sigma_t \\ \frac{d\sigma_x}{dx} + \frac{\tau}{h} &= 0 \quad (\text{Equilibrium condition})\end{aligned}\quad (5.23)$$

where:

$2a_0$ Width of excavation
 σ_r Stress in vertical direction
 σ_x Stress in horizontal direction
 τ Shear stress
 g Gravity
 h Half height of the strip

The stresses σ_x and σ_y depends only on direction x . There are no shear stresses. Due to this fact σ_x and σ_y are principal (normal) stresses. If dz approaches zero, the following equations can be established (Fig. 22):

$$\begin{aligned}\varepsilon_y = 0: & \quad \sigma_y = \sigma_y \quad (\sigma_y \cdot dx = \sigma_y \cdot dx) \\ \varepsilon_x = 0: & \quad \sigma_x \cdot 2 \cdot h - (\sigma_x + d\sigma_x) \cdot 2 \cdot h - 2 \cdot \tau \cdot dx \\ & \quad h \cdot d\sigma_x + \tau \cdot dx\end{aligned}\quad (5.24)$$

where:

$\varepsilon_x, \varepsilon_y$ Horizontal deformation

σ_x, σ_y ...Normal stresses

τ Shear stress

h Half height of the strip

According to the above mentioned formulas the following differential equation can be deduced :

$$\frac{d\sigma_z}{dz} + \frac{\tau}{a_0} = \rho \cdot g \quad (5.25)$$

where:

σ_zVertical stress

τ ...Shear stress

a_0 ...Half width of excavation

g ...Gravity

ρDensity

The limit state is defined by:

$$\tau = \lambda \cdot \tan(\phi) \cdot \sigma_r + C \quad (5.26)$$

where:

τ Shear stress

λ Coefficient of lateral pressure

σ_rVertical stress

ϕ Friction angle

C Cohesion

This finally leads to the following differential equation:

$$\frac{d\sigma_r}{dz} + \frac{\lambda \cdot \tan(\phi) \cdot \sigma_r}{a_0} = \rho \cdot g - \frac{C}{a_0} \quad (5.27)$$

By using the boundary condition: $\sigma_r(z=0) = 0$, the constant of integration A could be calculated and the final solutions can be obtained:

$$\sigma_r(z) = \frac{\rho \cdot g \cdot a_0 - C}{\lambda \cdot \tan(\phi)} \left[1 - e^{\left(-\lambda \cdot \tan(\phi) \cdot \frac{z}{a_0} \right)} \right] \quad (5.28)$$

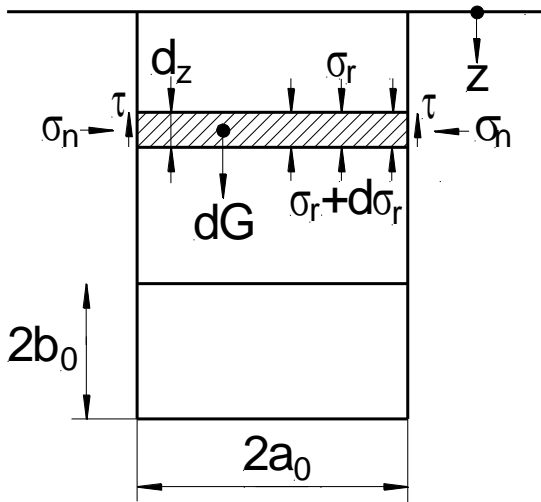


Fig. 21: Consideration of stresses acting on a infinitesimal strip

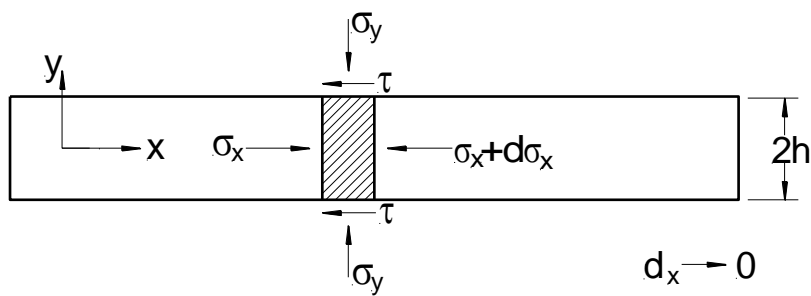


Fig. 22: Sketch to illustrate stress distribution at an infinitesimal small strip

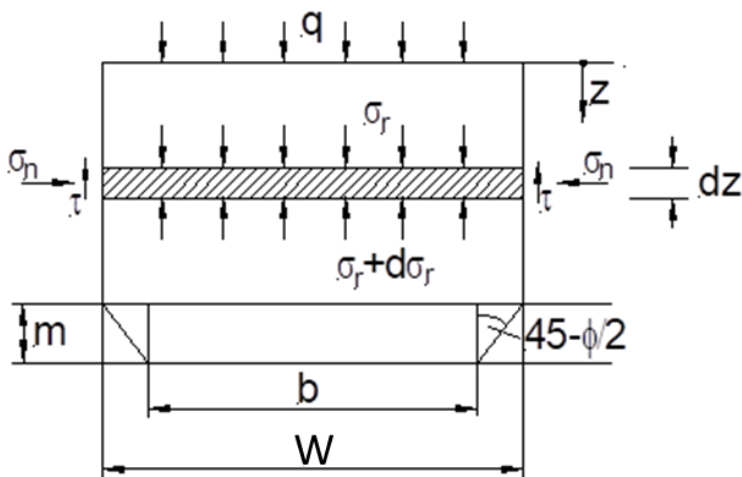


Fig. 23: Sketch for extended model of Terzaghi

a) Model Terzaghi (extended)

Terzaghi provided also an extension of his model by assuming that the failed area creates inclined sidewalls at the opening and the failed overburden area is becoming broader (

Fig. 23). The width of the developed failed area is given by:

$$W = 2 \cdot \left[\frac{b}{2} + m \cdot \tan\left(45^\circ - \frac{\phi}{2}\right) \right] \quad (5.29)$$

where:

W Width of failed area

b Width of excavation

m Excavation height

ϕ Friction angle

The limit state is characterized by the following equation:

$$\tau = \sigma \cdot \tan(\phi) + C = \sigma_h \cdot \tan(\phi) + C = \lambda \cdot \sigma_r \cdot \tan(\phi) + C \quad (5.30)$$

where:

τ Shear stress

λ Coefficient of lateral pressure

σ_r Vertical stress

σ_h Horizontal stress

ϕ Friction angle

C Cohesion

The force equilibrium at the stripe is:

$$0 = W \cdot (\sigma_r + d\sigma_r) - W \cdot \sigma_r + 2 \cdot \tau \cdot dz - W \cdot \rho \cdot g \cdot dz \quad (5.31)$$

At the limit state this results in the following equation:

$$0 = \frac{d\sigma_r}{dz} + 2 \cdot \lambda \cdot \sigma_r \cdot \frac{\tan(\phi)}{W} + \rho \cdot g - 2 \cdot \frac{C}{W} \quad (5.32)$$

After determination of integration constant the following solution is obtained:

$$\sigma_r = q \cdot e^{\left(-2 \cdot \lambda \cdot \frac{\tan(\phi)}{B} \cdot z\right)} + \left(\rho \cdot g - 2 \cdot \frac{C}{W}\right) \cdot \frac{W}{2 \cdot \lambda \cdot \tan(\phi)} \left[1 - e^{\left(-2 \cdot \lambda \cdot \frac{\tan(\phi)}{B} \cdot z\right)}\right] \quad (5.33)$$

6 Consequences of mining induced surface movements

Static ground movements

Damage on constructions depends not only on the surface movements itself, but also on the particular design properties of influenced objects. Different objects have different sensibilities in respect to surface movements. Tab. 5 evaluates the sensitivity of specific objects against certain ground movement parameters. Parameters without an influence on the object are coloured green and parameters with a significant impact on the object are coloured red and divided in three classes (low, medium and high impact).

Potential damage of objects is characterized by specific limit values. Most classifications are based on that of Budryk & Knothe (1956) and give object-based limit values for tilt (T_{limit}) critical radius (B_{limit}) and deformation (ϵ_{limit}). If specific ground movement parameters are below certain limit values, objects of a specific category do not suffer loss of functionality or stability. Nevertheless, smaller damages like small plastering fissures have to be expected even below these thresholds. Exemplary, Tab. 6 shows common limit values.

Tab. 5: Damage sensibility of various objects (green: □ no impact; red: □ low impact, □□ medium impact, □□□ high impact) (after Kratzsch, 1997)

Object	Subsidence	Tilt	Curvature	Displacement	Tension / Compression
House	□	□□	□□	□	□□
Office building	□	□	□□	□	□□
Terraced house	□	□□	□□	□	□□□
Machine	□	□□	□	□	□
Funnel	□	□□	□	□	□
Railway track	□□	□	□	□	□□
Road track	□	□	□	□	□□
Bridge	□□	□	□	□□	□
Sewer system	□□□	□	□	□	□□

Tab. 6: Limit values for surface movement parameters (after Budryk & Knothe, 1956)

Object category	T_{limit} [mm/m]	B_{limit} [km]	ε_{limit} [mm/m]	Examples
0	1	50	0.5	historical buildings, large-scale power plant
1	2.5	20	1.5	industrial complex, monuments
2	5.5	12	3	railroads, pipelines
3	10	6	6	low-rise buildings, roads, cables
4	15	4	9	storehouses, solid constructions
5	> 15	< 4	> 9	

Tab. 7: Limit values and their impact on objects (after Peng, 1992)

Parameter	Limit value	Damage	
T_{limit} [mm/m]	~10	construction is uncomfortable to occupy	
B_{limit} [km]	~50	damages on aboveground parts of the building	
ε_{limit} [mm/m]	2	concrete wall segments	damages on basement and basic structure
	3	masonry structures	
	10	cracks on roads (bitumen)	
	12	cracks in ground soil	

Tab. 8: Subsidence limits for different construction types

	Construction type	Subsidence limit S_{max} [mm]
Terzaghi & Peck (1961)	isolated footing	25
	base plate	50
Sowers & Sowers (1961)	frame construction	50 – 100
	brickwork	25 - 50
DIN EN 1997-1. Eurocode 7 (2008)	isolated footing	25
	base plate	50

Another set of thresholds and expected damages is proposed by Peng (1992) based on mining induced damages and protection measures (Tab. 7). To consider the subsidence s at constructions alone is less significant, but provides a first possibility for control and evaluation of a foundation. A distinct number of authors define rules and standards for tolerable subsidence dependent on type of foundation, static superstructure and ground conditions. Selected numbers are shown in Tab. 8. Detailed information about the interaction between constructions and subsoil including subsidence limits for several forms of structures are given in the work of Fischer (2009). Insurance companies use above-mentioned limit values to estimate payments of compensation for construction owners (Behrens & Minzemay, 2015).

Time-dependent ground movements

Mine-surveying analysis shows that induced damage on the surface depends not only on absolute movement parameters, but also on their evolution with time. The coherence of occurred deformation ε , deformation velocity $\dot{\varepsilon}$ and extraction rate v is shown in Fig. 24. Increasing extraction rates cause higher deformation velocities.

Dżegniuk & Sroka (1978), Sroka (1993), Dżegniuk et al. (1997) and Grün (1998) proposed specific limit values for time-dependent movement parameters (Tab. 9). These limits are subsidence velocity \dot{S}_{limit} , deformation velocity $\dot{\varepsilon}_{\text{limit}}$ and subsidence deficit Δsd . The subsidence velocity \dot{S}_{limit} will decrease if the excavation process stops at time t_1 . Regular subsidence move on after excavation delay at time t_2 . Subsidence that not occurred between time t_1 and t_2 is called subsidence deficit Δsd (Fig. 25). Białek (1995) derived another correlation between time-dependent ground movement and object damages based on a statistical approach. He connects static and dynamic stress on constructions by effective deformation ε_{eff} :

$$\varepsilon_{\text{eff}} = 0.31 \cdot \varepsilon_{\text{max}} + 0.43 \cdot \dot{S}_{\text{max}} \quad (6.1)$$

where:

ε_{eff} Effective deformation

ε_{max} ... Maximum deformation

\dot{S}_{max} ... Maximum subsidence velocity

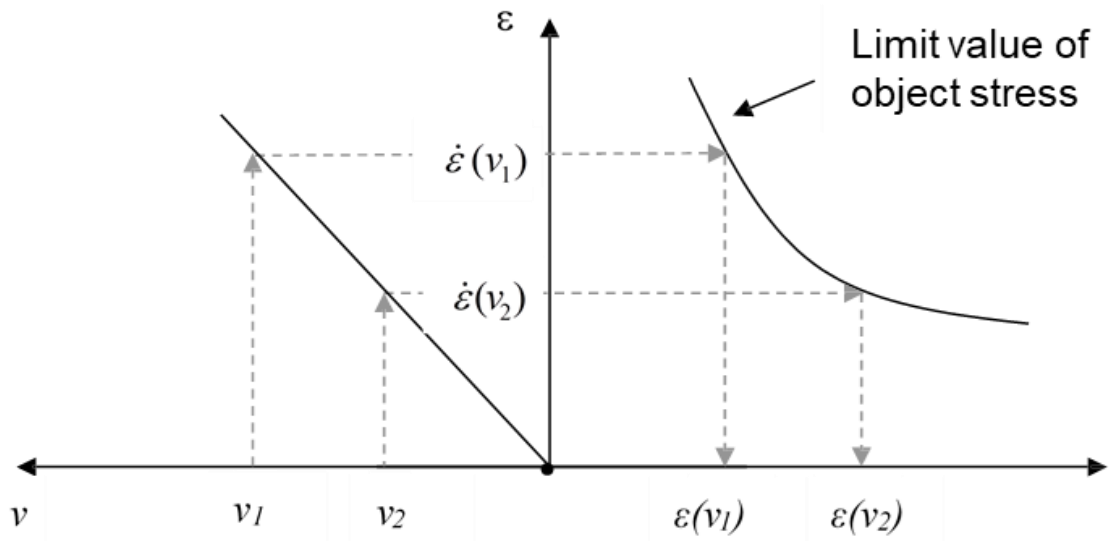


Fig. 24: Relationship between extraction rate, deformation velocity and their influence on object damage (after Sroka, 1993)

Tab. 9: Limit values for time-dependent ground movement parameters (after Sroka, 2003)

Object category	\dot{S}_{limit} [mm/day]	$\dot{\epsilon}_{\text{limit}}$ [mm/m/day]	Δsd [mm]	Examples
0	1	0.005	1	historical buildings, large-scale power plant
1	3	0.015	2.5	industrial complex, monuments
2	6	0.03	5	railroads, pipelines
3	12	0.06	10	low-rise buildings, roads, cables
4	18	0.1	15	storehouses, solid constructions
5	> 18	> 0.1	> 15	

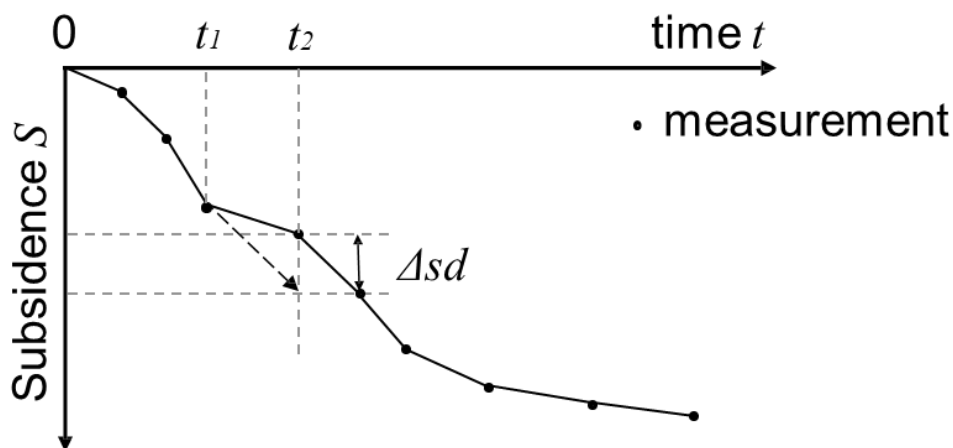


Fig. 25: Effect of an excavation delay on the subsidence progress (after Zimmermann, 2011)

7 Numerical Models

Frequently used numerical methods for the simulation of subsidence and sinkholes are the Finite Element Method (FEM), the Finite Difference Method (FDM) and the Discrete Element Method (DEM) incl. particle based methods. The following three simple examples show the potential of numerical simulation techniques to predict subsidence trough or sinkholes based on geomechanical constitutive laws and parameters. In contrast to geodetic, mine-surveying based, empirical or statistical methods, numerical methods can work without any pre-existing local subsidence or sinkhole data. They need however rock mass strength and stiffness parameters.

Example 1: Numerical simulation of continuous subsidence above an underground coal mine

An underground coal mine may be located in a layered rock mass as shown in Fig. 26. The excavation has a width of 600 m in x - and y -direction. The mining height is 4 m and it takes place at a depth of 503 m to 507 m. Using Eq. 10 to determine the critical width give us a value of $w_c = 627.14$ m. The excavation does not reach the critical width, therefore the model provides a subcritical state. Due to the symmetry of model and boundary conditions only a quarter of the model is simulated to speed up the calculation time. The obtained subsidence after extraction of coal is illustrated in Fig. 27 and 28. Also the typical subsidence-trough of continuous subsidence is shown until final closure of the opening. To predict subsidence profiles at the surface, in parallel to the numerical simulations the profile functions according to Eq. 10, 12 and 13 are used. Fig. 29 shows the subsidence profiles obtained from numerical calculations (red) and the analytical solutions (black dotted and blue dotted) by using the exponential functions (Eq. 14).

In reality the begin of the subsidence trough depends on the precision of the survey. The used accuracy reflects the determination of the half width of subsidence trough w_s , which is necessary for the analytical calculation. To illustrate this effect two levels of accuracy (± 10 mm and ± 1 mm) of surveying are used for the analytical solution. It becomes obvious, that the analytical solution fits better with the numerical simulations by increasing the precision of the survey (blue dotted line). Analytical solutions for hyperbolic functions (Eq. 16 and 17) are shown in Fig. 30. As visible from Fig. 29 and Fig. 30, the exponential function is better suited for the considered constellation.

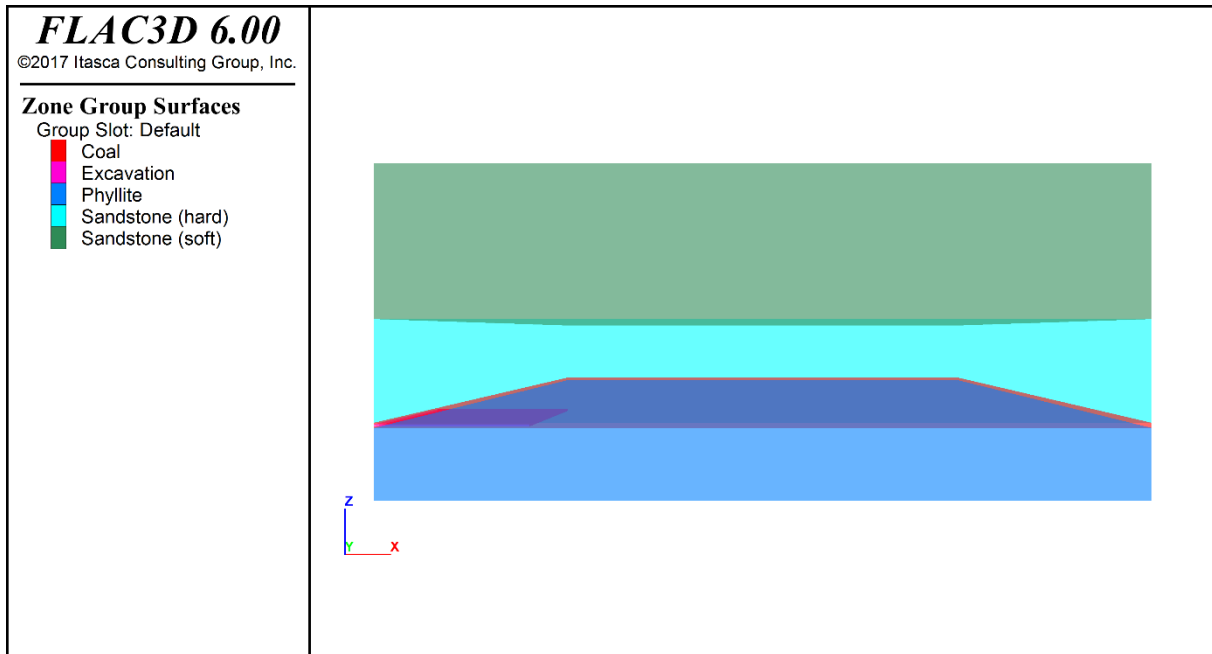


Fig. 26: Numerical model set with layers (excavation of a coal bed in the underground)

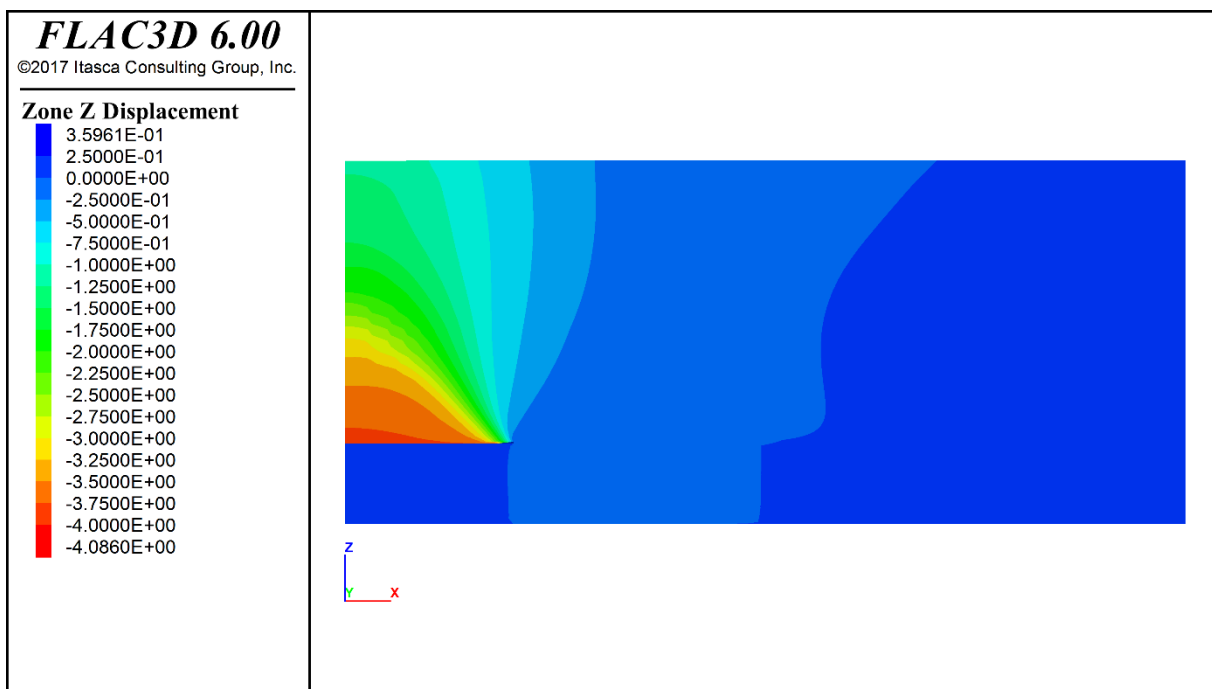


Fig. 27: Contour plot of vertical displacements (in m) for a cross section

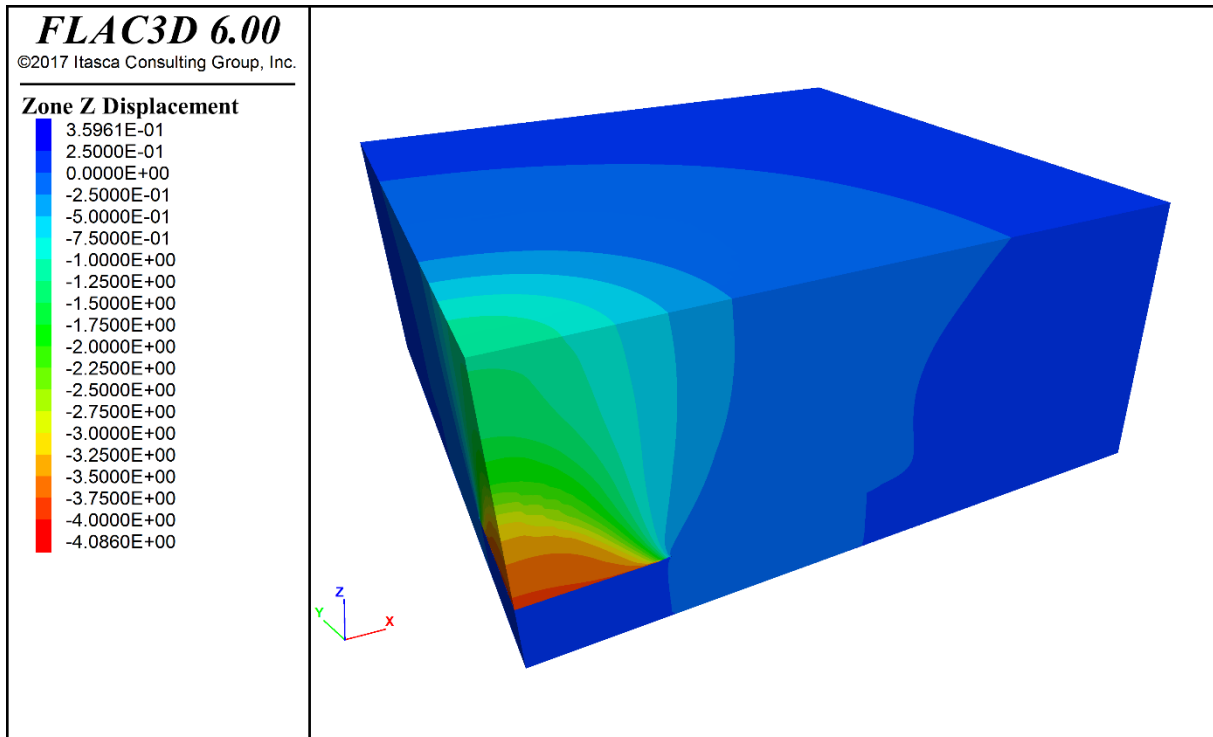


Fig. 28: Contour plot of vertical displacements (m)

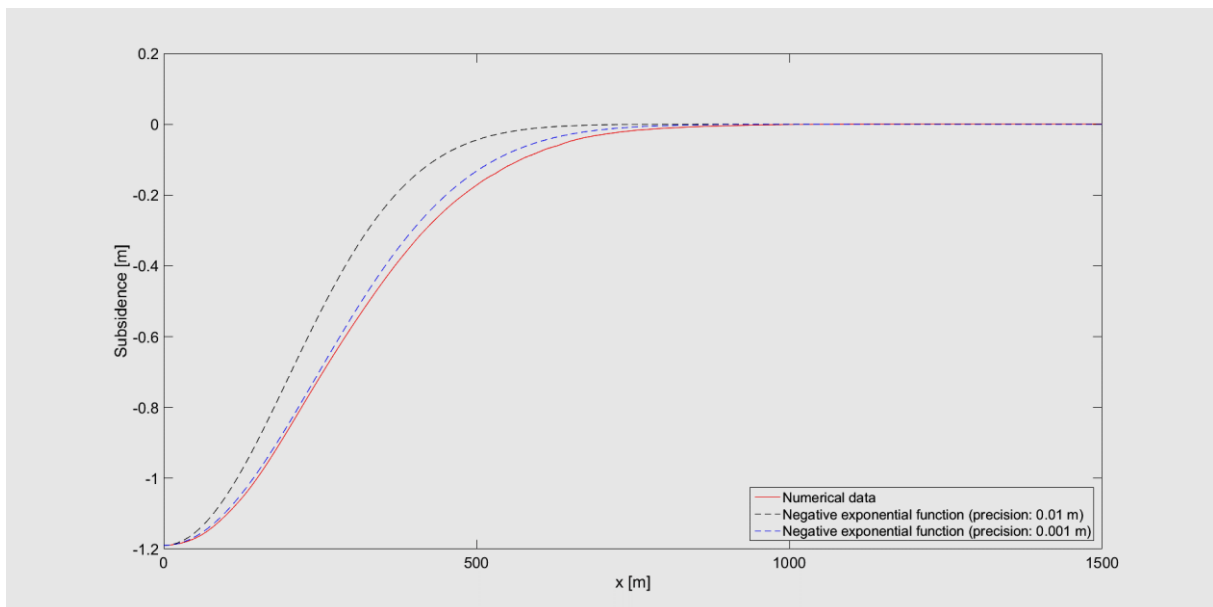


Fig. 29: Numerical data and analytical solution by use of an exponential function with different survey precisions

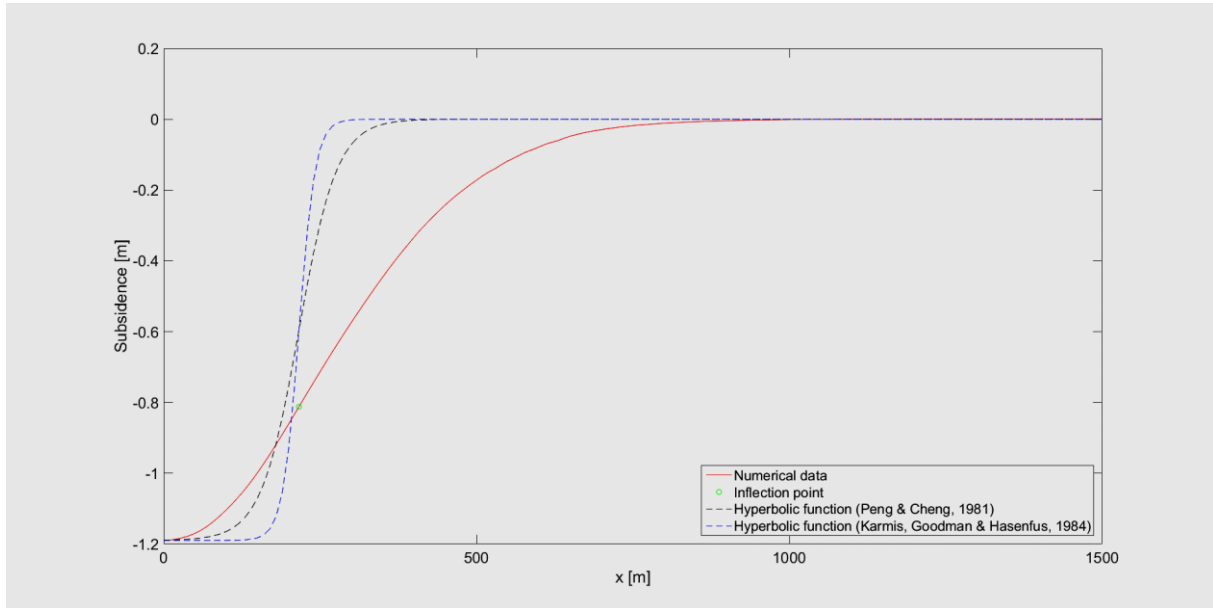


Fig. 30: Numerical data and analytical solution by use of hyperbolic functions

**Example 2: Numerical simulation of sinkhole with an continuum approach
(Shiau et al., 2016)**

This 2-dimensional example is based on the strength-reduction technique to predict safety factors and potential shape of sinkhole.

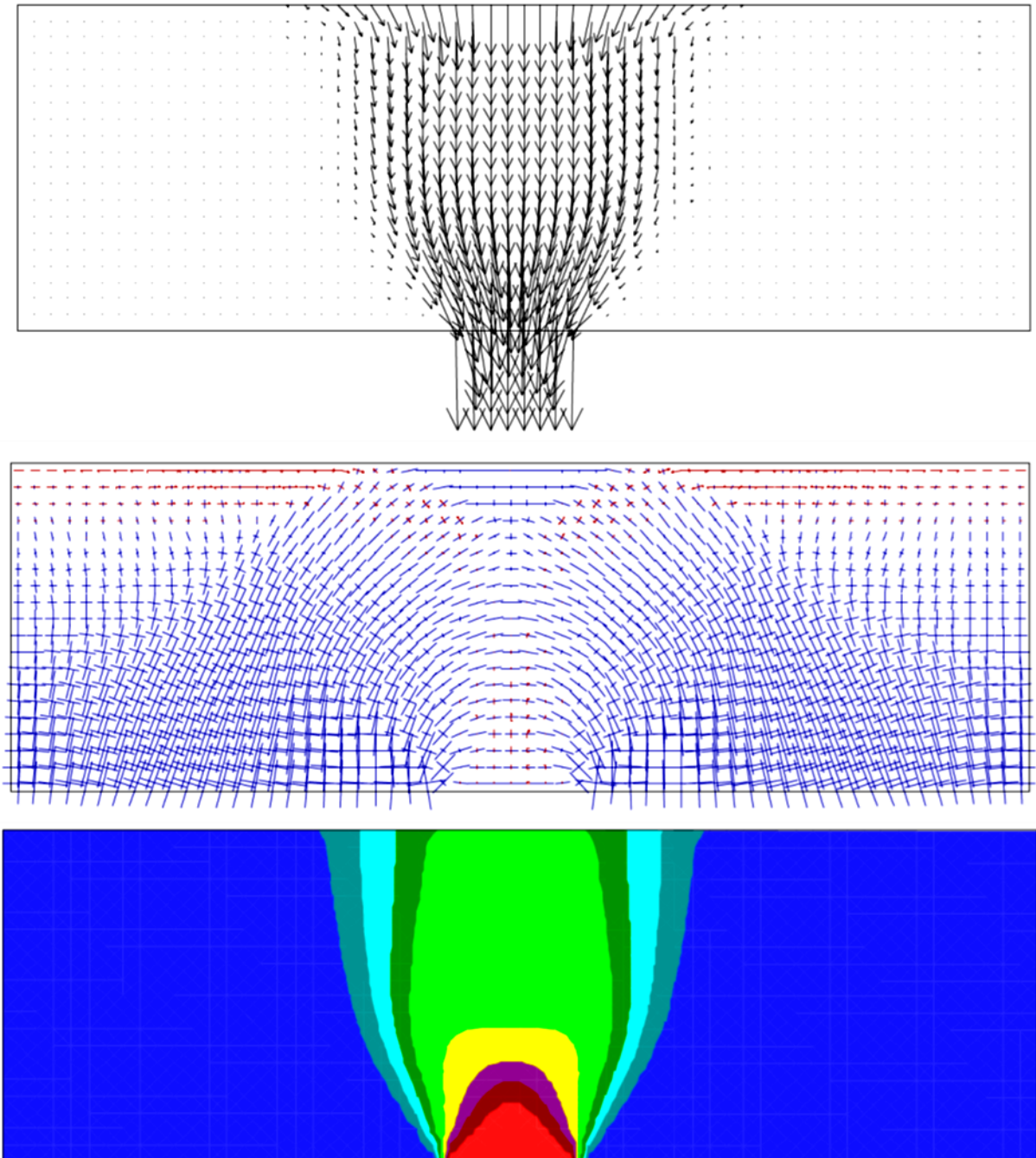


Fig. 31: Simulation of onset of sinkhole development due to strength reduction (top: displacement vectors, middle: principal stresses, down: displacement contours)

**Example 3: Numerical simulation of sinkhole with a discontinuum approach
(Coudron et al., 2006)**

The development of sinkholes is a highly discontinuum mechanical process of damage, fracturing and mass transport. Therefore, continuum mechanical approaches have limited capabilities to duplicate this process. Discrete element or particle based approaches can be used to simulate this process as shown by this example, which couples a particle code (PFC) and a continuum code (FLAC). Fig. 32 shows an interim stage during the sinkhole evolution and Fig. 33 to Fig. 35 as well as Tab. 9 document, that such a procedure is able to duplicate the movements in a quite realistic manner.

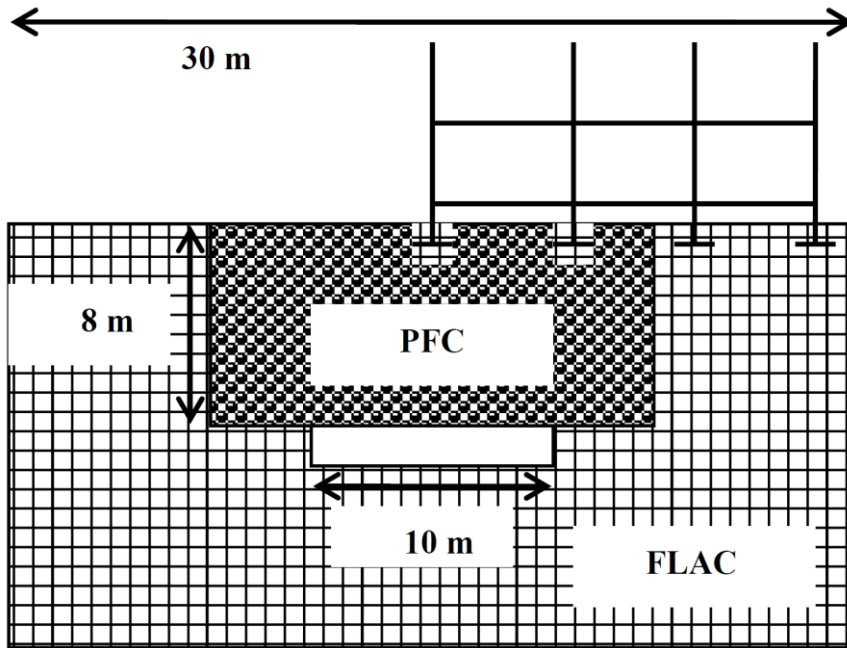


Fig. 32: Model set-up for 2-dimensional continuum-discontinuum coupled simulation of a sinkhole process in a layered rock mass

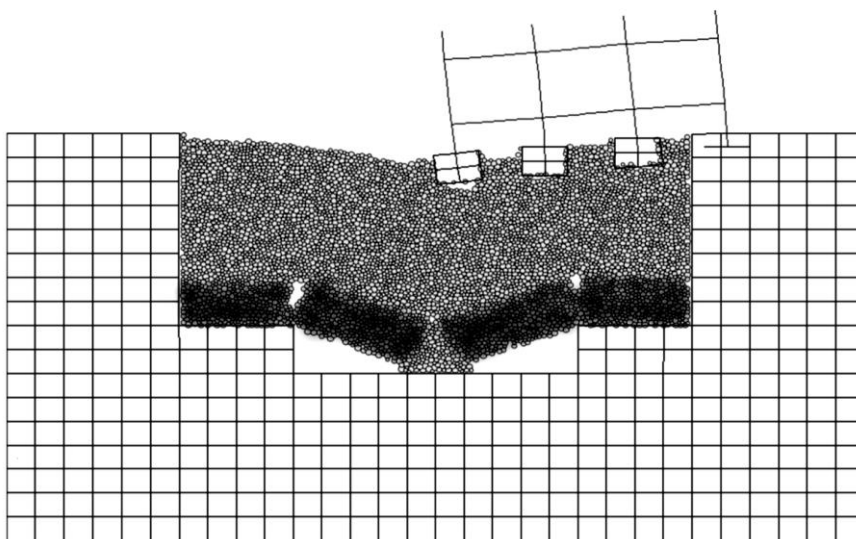


Fig. 33: Interim stage of sinkhole development with foundation interaction

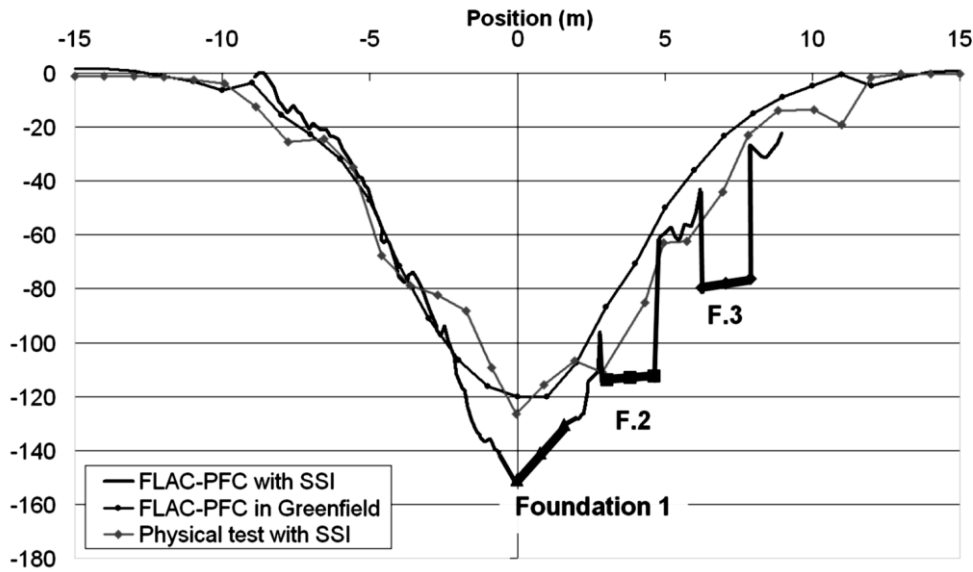


Fig. 34: Comparison between predicted and measured settlement values

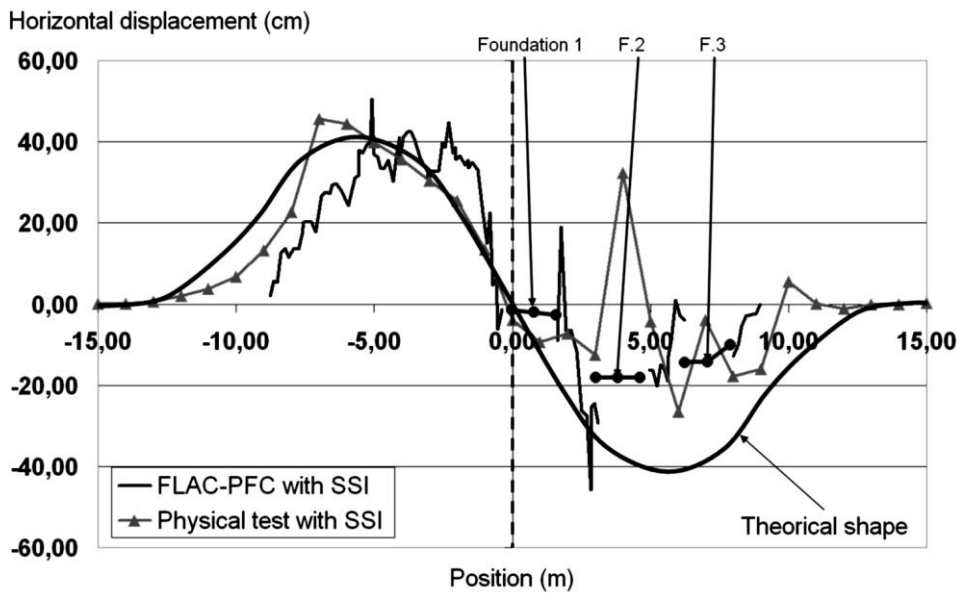


Fig. 35: Comparison between predicted and measured horizontal displacements

Tab. 10: Comparison between predicted and measured values

Characteristic	Physical test with SSI	FLAC-PFC in greenfield	FLAC-PFC with SSI
S_{max}	127 cm	120 cm	151 cm
i	~4.5 m	~4 m	~4 m
% of V_{cavity}	64%	58%	54%
Maximum slope	35%	24%	34%
Maximum slope on the building	~18%	~15.3%	~11%
Situation (span)	F ₂ -F ₃	F ₂ -F ₃	F ₂ -F ₃

Example 4: Numerical simulation of sinkhole over brine-filled caverns with a discontinuum approach (Minkley & Lüdeling, 2020)

Sinkholes over deep brine-filled caverns can occur in case of integrity loss of barriers due to percolation processes in conjunction with initiation of fluid pressure on pre-existing joints. Fig. 36 illustrates some spectacular sinkholes over deep brine caverns. Discontinuous hydro-mechanical coupled modelling under consideration of the percolation concept allows to simulate the sinkhole process. Fig. 37 and 38 show numerical simulation results, which document, that cavern span and lateral stress have important influence on sinkhole development. The authors concluded that sinkhole formation over brine-filled caverns requires the following conditions:

- sufficiently large caverns without salt back, i.e. with hydraulic connection between the cavern and the overburden,
- jointed overburden with moderate to low shear strength,
- moderate to low horizontal (confining) stresses in the overburden,
- fluid pressure on the overburden joints.

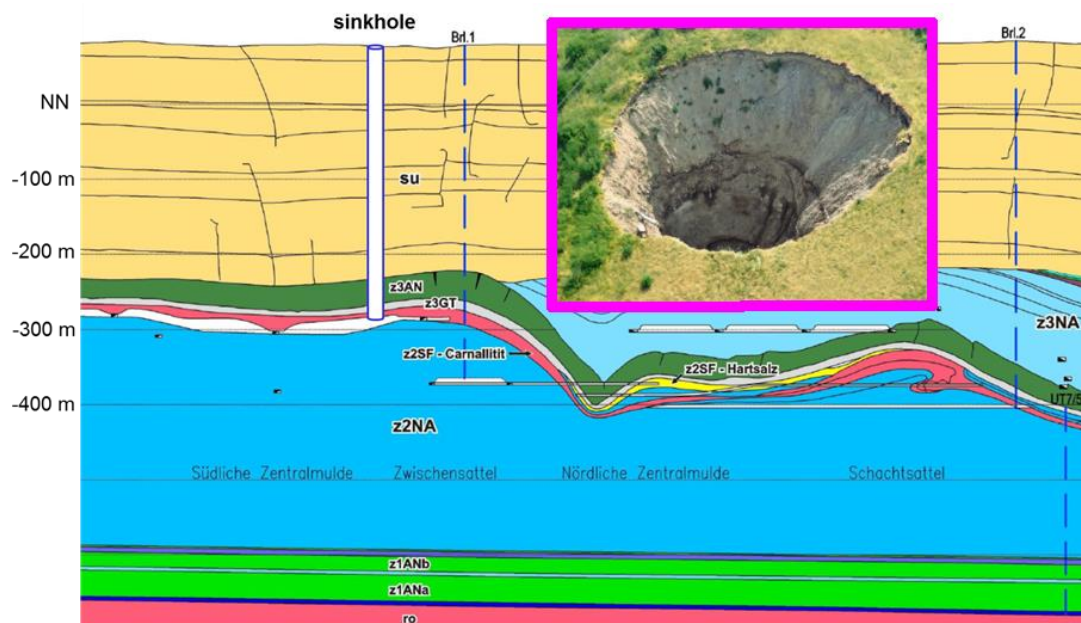


Fig. 36: Selected sinkholes over brine caverns (top: Louisiana, USA; bottom: Central Germany)

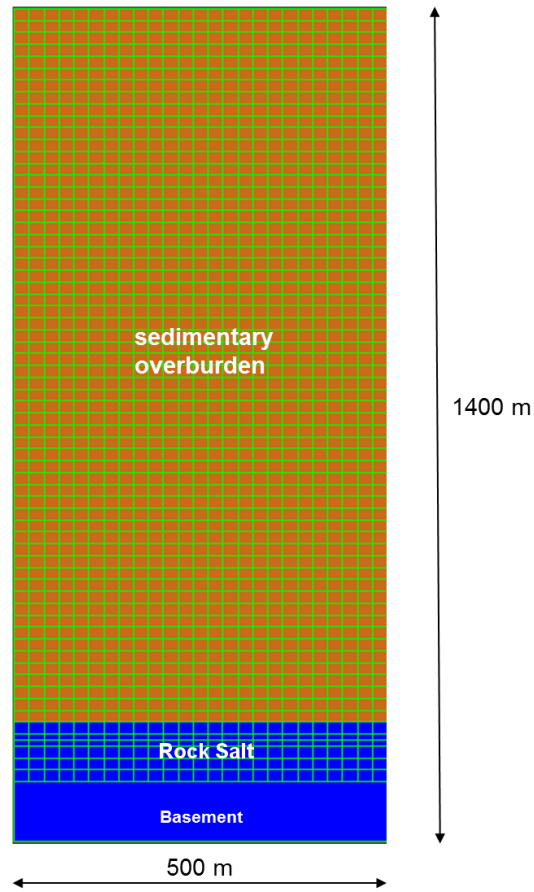


Fig. 37: Numerical model setup

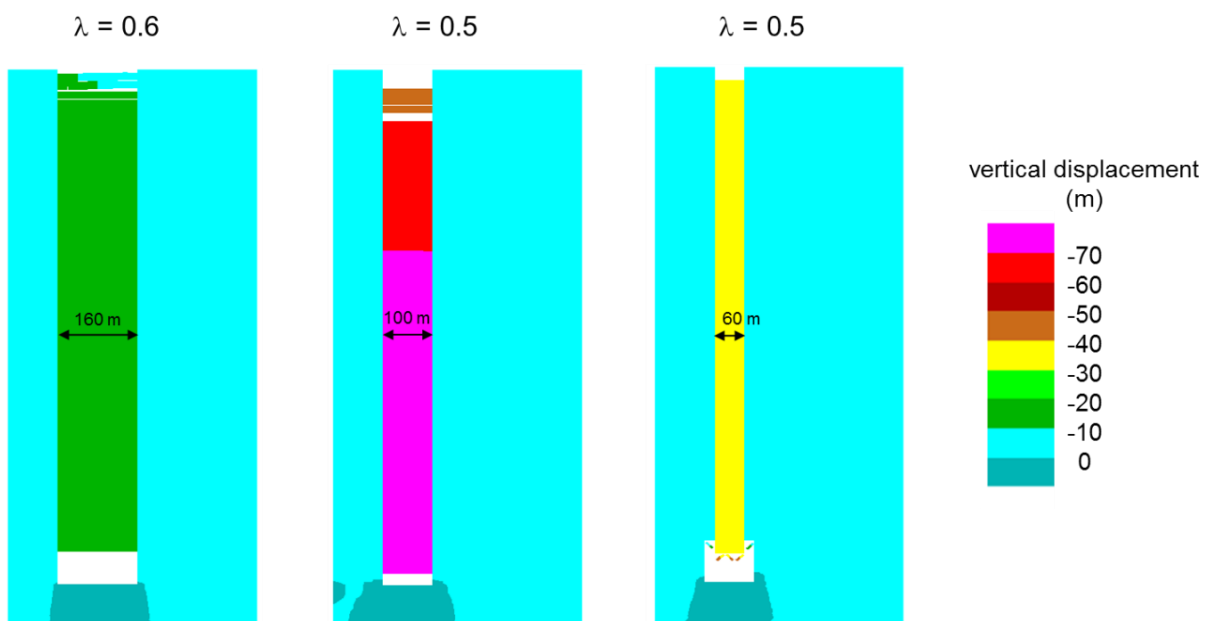


Fig. 38: Sinkhole scenarios depending on cavern span and horizontal earth pressure λ

Example 5: Numerical simulation of sinkhole using a particle based approach discontinuum approach (Song & Konietzky, 2019)

Fig. 39 illustrates the numerical simulation of a sinkhole evolution at drift connection (room and pillar mining). The mass flow into the drifts including the bulk cone formation is well duplicated.

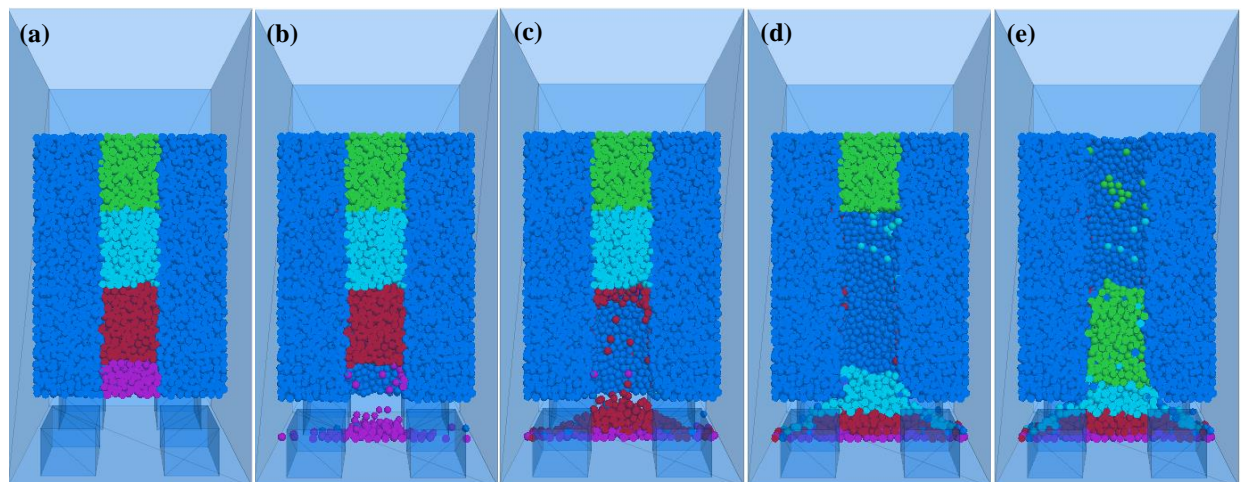
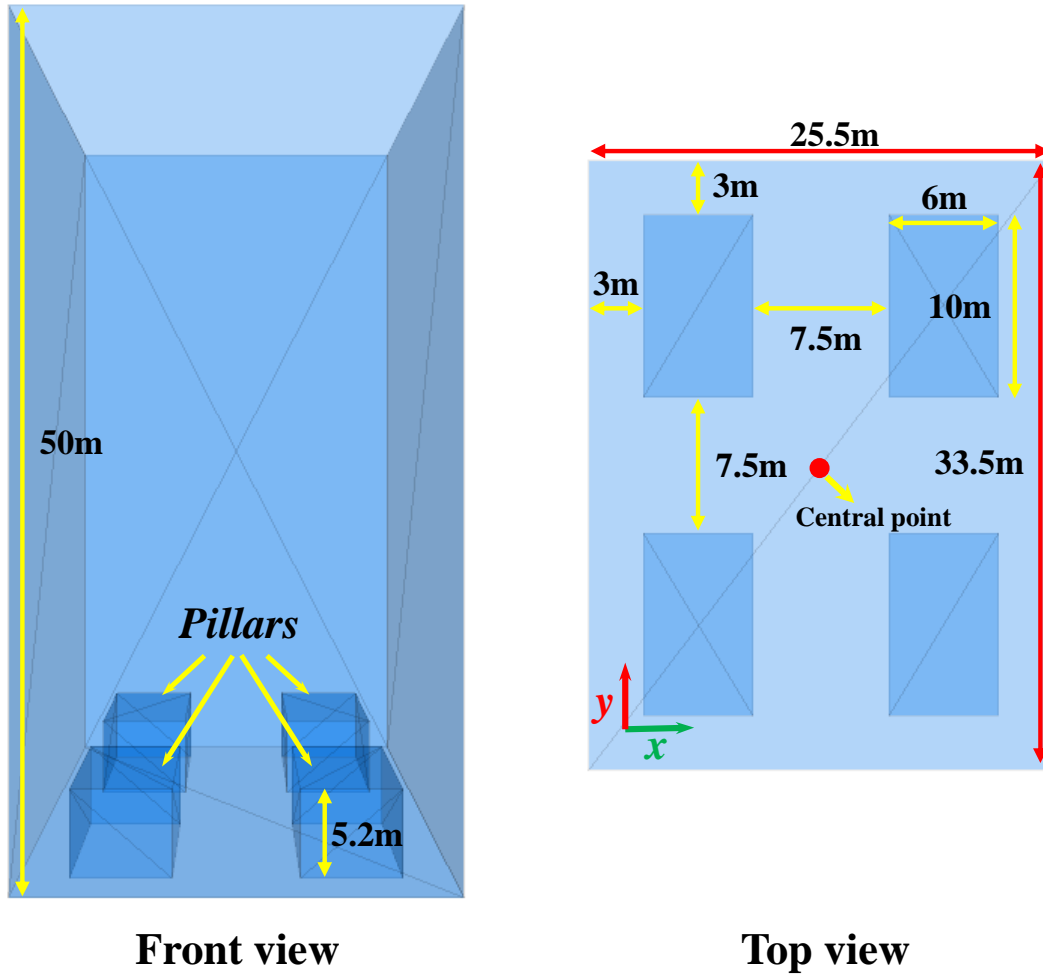


Fig. 38: Sinkhole evolution above a drift intersection simulated with a particle based approach

8 References

- Behrens, U., & Minzemay, B. (2015). *Bergschaden - Minderwert - Schief lagen*.
- Białek, J. (1995). Der Einfluss der Bodenbewegungsgeschwindigkeit auf die Schäden an Gebäuden (polish language). *Schule des Untertägigen Bergbaus*.
- Bierbaumer, A. (1913). *Die Dimensionierung des Tunnelmauerwerkes*. Leipzig: W. Engelmann.
- Brady, B., & Brown, E. (2004). *Rock Mechanics for underground mining*. Dordrecht: Kluwer Academic Publishers.
- Budryk, W., & Knothe, S. (1956). Zasady klasyfikacji terenów Górnośląskiego Okręgu Przemysłowego ze względu na możliwość ich zabudowy. *PAN – Komisja Mechaniki Górnotworu, Biuletyn Nr. 4*.
- Dżegniuk, B., & Sroka, A. (1978). Der Einfluss der Abbaugeschwindigkeit auf die Gebirgs- und Bodenbewegungen. *Wissenschaftliches Symposium der polnischen Akademie der Wissenschaften*. Katowice (Poland).
- Dżegniuk, B., Hejmanowski, R., & Sroka, A. (1997). Ocena zagrożenia obiektów budowlanych na terenach górniczych z uwzględnieniem przebiegu deformacji w czasie. *10. ISM Congress*. Perth (Australia).
- Clostermann, M. et al. (2020): Einwirkungsrelevanz des Altbergbaus, Bemessung von Einwirkungs- und Gefährdungsbereichen und Einfluss von Grubenwasserstandsänderungen, Gutachterliche Stellungnahme im Auftrag der Bezirksregierung Arnsberg, Abteilung Bergbau und Energie NRW
- Eckart, D. (August 1972). Arten und Ursachen von Schäden an stillgelegten Bergwerksanlagen. *Neue Bergbautechnik*(Heft 8).
- Eckart, D. (1973). Ergebnisse von Untersuchungen über Schäden an stillgelegten Bergwerksanlagen. *Freiberger Forschungshefte*(256).
- Fenk, J. (1979). Eine Theorie zur Entstehung von Tagesbrüchen über Hohlräumen im Lockergebirge. *Dissertation*. Freiberg: TU Bergakademie Freiberg.
- Fenk, J. (1981). *Eine Theorie zur Entstehung von Tagesbrüchen über Hohlräumen im Lockergebirge - (FFH A 639)*. Leipzig: VEB Deutscher Verlag für Grundstoffindustrie.
- Fenk, J. (1984, November). Berechnung von Tagesbrüchen. *Neue Bergbautechnik*(Heft 11), pp. 414-416,425.
- Fenk, J. (1994). Bergschadenprobleme in Ostdeutschland. *Das Markscheidewesen*(101), pp. 18-23.
- Fenk, J. (2000). *Tagesbrüche über Hohlräumen im Lockergebirge mit geneigter Schichtlagerung*. TU Bergakademie Freiberg. Freiberg: Institut für Markscheidewesen und Geodäsie.
- Fischer, D. (Oktober 2009). Dissertation. *Interaktion zwischen Baugrund und Bauwerk - Zulässige Setzungsdifferenzen sowie Beanspruchung von Bauwerk und Gründung* -. Schriftenreihe Geotechnik Universität Kassel (Prof. Dr-Ing. H.-G. Kempfert).

- Grün, E. (1998). Planung von Hochleistungsstreben unter Berücksichtigung der Umweltverträglichkeit in Bezug auf Bauwerksprophylaxe und Bergschadenserwartung. (T. B. (Germany), Hrsg.) *Freiberger Forschungshefte*.
- Jarosz, A. (1975). Ein Modell zur Entstehung von Tagesbrüchen. *Geodäsie, Polnische Akademie der Wissenschaften*, S. 65-82.
- Karmis, M., Goodman, G., & Hasenfus, G. (1984, August 6-8). Subsidence Prediction Techniques for Longwall and Room and Pillar Panels in Appalachia. *Proceedings of the 2nd International Conference on Ground Control in Mining*, pp. 311-328.
- Kratzsch, H. (1997). *Bergschadenkunde*. Berlin, Heidelberg: Springer-Verlag.
- Lerche, I., & Lempp, C. (2002). Methods for Estimating Associated Risks of Sinkhole Occurrences: A Demonstration Using Available Data from the Rhur Valley Region of Germany. *Environmental Geosciences*(9), S. 173-183.
- Lin, Y. (2017). Bericht. *Abandoned Mines and Sinkhole Risks*. TU Bergakademie Freiberg.
- Liszkowski, J. (1973). Bemerkungen über die Geomechanik von Erdfällen. *Proc. Congr. Ing.-Geol, Erdfälle und Bodensenkungen* (S. 1-5). Hannover: IAEG.
- Luo, Y., & Peng, S. (1997). Subsidence Prediction Influence Assessments and Damage Control. *Proceedings of the 16th International Conference of Groundcontrol in Mining* (S. 50-57). Morgantown, WV, USA: West Virginia University.
- Meier, G. (November 1978). Zum Problem von Tagesbruchanalysen in Altbergbaugebieten aus der Sicht der praktischen Bergsicherungsarbeiten. *Neue Bergbautechnik*, S. 639-643.
- Meier, G. (2001). Numerische Abschätzung von Tagesbruchgefährdungen in Altbergbaugebieten. *13. Nationale Tagung für Ingenieurgeologie, Sonderband Geotechnik*, S. 95-100. Karlsruhe.
- Meier, J. (2003). Diplomarbeit. *Statistische Analyse von tagesbrüchen über Abbaufeldern des Braunkohlen-Tiefbaus und ein Versuch ihrer numerischen Simulation mit dem Programm FLAC*. Freiberg: TU Bergakademie Freiberg.
- Meier, J. & Meier, G. (2005): *Modifikation von Tagesbruchprognosen nach G. Meier*, Geotechnik, 2: 1-6
- Minkley, W. & Lüdeling, C. (2020): Sinkholes over deep caverns, Proc. 49. Geomechanics Colloquium, H. Konietzky (ed.), Geotechnical Institute, TU Bergakademie Freiberg, 20 p.
- National Coal Board. (1975). *Subsidence Engineers Handbook*. London: National Coal Board Mining Dept.
- Pariseau, W. (2012). *Design Analysis in Rock Mechanics*. London: Taylor & Francis Group.
- Peng, S. (1992). *Surface Subsidence Engineering; Society for Mining*. Colorado (USA): Metallurgy and Exploration Inc.

- Peng, S. S. (2008). *Coal Mine Ground Control*. Morgantown, West Virginia, USA: Department of Mining Engineering, College of Engineering and Mineral Resources, West Virginia University.
- Peng, S., & Cheng, S. (1981, May). Predicting Surface Subsidence for Damage Prevention. *Coal Mining and Processing*, pp. 84-95.
- Penzel, M. (1980). Bemerkungen zu Erdfallgenese in Auslaugungsgebieten aus der geomechanischen Sicht. *Neue Bergbautechnik*, S. 15-19.
- Penzel, M. (1981). Probleme der Prognose und Deutung von Erdfällen unter besonderer Berücksichtigung der Verkarstung im südöstlichen Harzvorland. *Dissertation*. Freiberg: TU Bergakademie Freiberg.
- Protodjakonov, M. (1926). *Materials for a fixed position of mining operations, Part I. Mining operations*. Publication of the TsK of miners.
- Reuter, F., & Waldmann, J. (1978). Das Karstproblem in der Ingenieurgeologie. *Dissertation*. Freiberg: TU Bergakademie Freiberg.
- Salustowicz, A. (2009). *Outline of Rock Mass Mechanics*. Krakow: AGH University of Science and Technology Press.
- Song, Z., Konietzky, H. (2019): Sinkhole simulation, unpublished study, Chair for Rock Mechanics, TU Bergakademie Freiberg
- Sowers, G., & Sowers, G. (1961). *Introductory soil Mechanics and Foundations*. New York: The Macmillan Comp.
- Sroka, A. (1993). Zum Problem der Abbaugeschwindigkeit aus bergschadenkundlicher Sicht. *Tagungsband Szkoła Eksploatacji Podziemnej*. Ustron (Poland).
- Sroka, A. (2003). Der Einfluss von Hochleistungsstreben auf das Gebirge und die Tagesoberfläche. *Glückauf- Forschungshefte*.
- Terzaghi, K. (1943). *Rock defects and load on tunnel supports*. New York: John Wiley & Sons.
- Terzaghi, K., & Peck, R. (1961). *Die Bodenmechanik in der Baupraxis*. Springer-Verlag.
- Zimmermann, K. (2011). Prognose und bergschadenkundliche Analyse dynamischer Bodenbewegungen durch oberflächennahen Steinkohlenbergbau in den USA. *Dissertation*. TU Bergakademie Freiberg.